DEPARTMENT OF THE INTERIOR
U.S. GEOLOGICAL SURVEY

TO ACCOMPANY MAP I-1803-B

MAP SHOWING ANALYSIS OF LINEAR FEATURES FOR MINERAL ASSESSMENT IN THE DILLON 1° X 2° QUADRANGLE, IDAHO AND MONTANA

By

T.L. Purdy and L.C. Rowan

INTRODUCTION

This study was undertaken in the Dillon, Montana-Idaho 1° X 2° quadrangle as part of the Conterminous U.S. Mineral Assessment Program (CUSMAP) by the U.S. Geological Survey (USGS). The purpose of the study was to derive structural information from Landsat multispectral scanner (MSS) images and a mosaic of proprietary side-looking airborne radar (SLAR) images. This information, along with the locations of exposures of hydrothermally altered rocks (Segal and Rowan, 1989), can aid in the mineral resource assessment of the quadrangle.

The structural information obtained from interpretation of the MSS and SLAR images consists mainly of linear features, and subordinately of arcuate features. Linear features are defined as distinct linear to slightly curvilinear elements mappable on MSS and SLAR images. They generally represent linear segments of streams, ridges, or terminations of topographic features. However, they may also represent tonal variations. A lineament is defined as an alignment of linear features that exhibits a pattern which is distinct from that of adjacent linear features (O'Leary and others, 1976). We assume that most of the linear features in the Dillon quadrangle reflect underlying structurally controlled elements, such as fractures, faults, dikes, and alignments of fold axes. Linear features such as obvious layered strata and cultural features were excluded during mapping and compilation. Therefore, lineaments derived from the linear features are believed to represent simple or compound structural zones.

Arcuate features range from distinctly curved but open features to features that are ellipsoidal in form. Arcuate features may be attributed to a variety of causes. In igneous environments they may be associated with either doming related to intrusive activity or to caldera collapse related to extrusive activity. In sedimentary terrains such features may be attributed to folding or doming due to tectonic activity or diapiric movements of evaporites. Glaciation also commonly produces arcuate features.

This report describes the geologic setting of the Dillon quadrangle and the procedures used in mapping the linear and arcuate features. The analysis of the linear features concentrates on their azimuthal trends, lengths, and areal densities. The results of these analyses are combined with the distribution of exposures of altered rocks (Segal and Rowan, 1989) in order to construct a composite map that shows relative mineral potential in the quadrangle based on these data alone.

Physiography and Vegetation

The Dillon 1° X 2° quadrangle lies in southwestern Montana and the adjacent part of east-central Idaho (fig. 1). The rugged terrain consists of mountain ranges separated by broad, open basins; elevations range from approximately 1,370 m to 3,350 m. The area consists of mountain ranges separated by broad, open basins. Vegetation in the basins is predominately sagebrush (*Artemisia tridentata*), rabbitbrush (*Chrysothamnus* sp.), and a variety of grasses and forbs. The ranges support Douglas fir (*Pseudotsuga menziesii*), lodgepole pine (*Pinus contorta*), and subalpine fir (*Abies lasiocarpa*) in the higher elevations.

Geology

The following discussion comes largely from Ruppel and others (1981). The area is underlain by rocks ranging in age from Precambrian to Tertiary (fig. 2). The quadrangle contains several major thrust plates which were transported eastward during late Early to Late Cretaceous time (Ruppel and others, 1981) and are characterized by distinctive lithologies and structural styles. The plates (from west to east) are the Medicine Lodge plate, the Grasshopper plate, and the frontal fold-and-thrust zone. The craton lies at the eastern boundary of the quadrangle.

The Medicine Lodge plate is composed primarily of Proterozoic rocks and a sequence of Paleozoic sedimentary rocks. The Grasshopper plate, structurally beneath the Medicine Lodge plate and above the frontal fold-and-thrust zone, consists of Proterozoic, Cambrian, and Devonian sedimentary rocks. The frontal fold-and-thrust zone is the leading edge of the thrust belt in southwestern Montana and consists of Paleozoic and Mesozoic sedimentary rocks. The plates were intruded during the Late Cretaceous and Tertiary by batholithic rocks related to both the Idaho and Boulder batholiths. These episodes of intrusion resulted in deformation to the host rocks. The ranges were faulted during the Tertiary in a manner similar to the basin-range structure to the south (Reynolds, 1979); Tertiary and Quaternary sediments have filled the basins. Pleistocene glaciation has modified the topography at higher elevations.

MAPPING PROCEDURES

Initially, linear features were mapped on approximately 1:300,000-scale, contrast-enhanced,

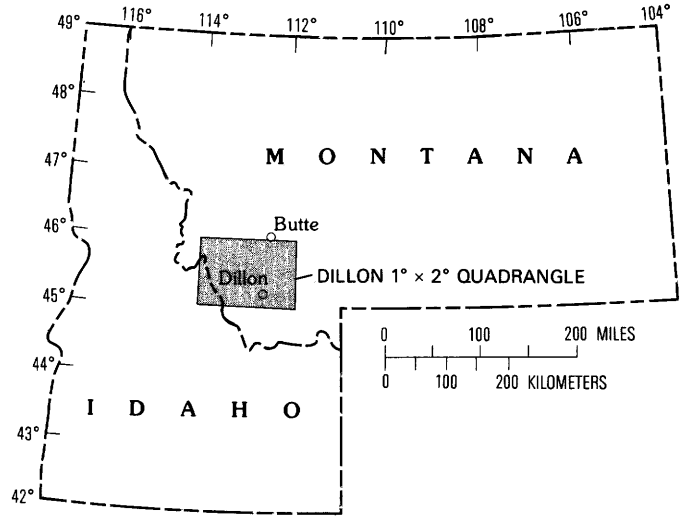
49°
116°
114°
112°
110°
108°
106°
104°
48°
47°
46°
45°
44°
43°
42°
M O N T A N A
Butte
Dillon
DILLON 1° × 2° QUADRANGLE
0 100 200 MILES
0 100 200 KILOMETERS
I D A H O

INDEX MAP

Landsat MSS band 5 (0.6-0.7 micrometers) and band 7 (0.8-1.1 micrometers) images, and on 1:250,000-scale MSS color-infrared composite images. Three MSS scenes were needed to cover the quadrangle: scene 2553-17331, acquired July 28, 1976; and scenes 1790-17361 and 1791-17415, acquired September 22, 1974.

Subsequently, we mapped linear features on a mosaic of 1:250,000-scale SLAR images. Only those features that were not delineated on the MSS images were mapped on the mosaic in order to avoid redundant data. The SLAR data were recorded during December 1979 with X-band frequency (2.4-3.8 cm), a 20-45 degree depression angle, and westward illumination. The low depression angle resulted in extensive shadows on west-facing slopes in high-relief areas, and this shadowing tended to obscure linear features. Shadows occurred on northwest-facing slopes in the MSS images (fig. 3), although they were not as severe as in the SLAR images. Interpretation of the SLAR image, which had a 10-meter resolution, provided information not available from the 79-meter resolution of the MSS images. In addition, use of the SLAR image aided in alleviating the sun-angle (solar elevation above the horizon and azimuth) bias that has been noted in MSS linear feature data in previous studies (Rowan and Purdy, 1985).

The linear features were digitized to facilitate further analysis. Curvilinear features were subdivided into a series of straight segments that were digitized sequentially.

ANALYSIS OF LINEAR FEATURES

Linear features have three principal characteristics: areal density, azimuthal trend, and length. We analyzed each of these characteristics individually and in several combinations. Initially, the linear features mapped on the MSS and SLAR images were evaluated as two separate groups in order to illustrate differences in areal distribution that are primarily related to illumination differences, but spatial-resolution differences also play a role. Most of the analysis was conducted subsequently using these two data sets together, because the extensive shadows in the SLAR mosaic resulted in incomplete coverage of the linear features.

Areal Density

The distributions of linear features mapped on the MSS and SLAR images are shown in figures 4 and 5, respectively. In general, the linear features on the MSS images appear to be more uniformly distributed because of the more extensive shadowed areas in the SLAR image. In the MSS map (fig. 4), the highest densities of linear features occur in the Pioneer and Beaverhead Mountains and the Bitterroot Range, with isolated areas of high density in the Ruby Range and the southeastern part of the Highland Mountains (see fig. 1). The relatively low density of features mapped on the western slopes of the Tobacco Root Mountains and southern Bitterroot Range is due partly to shadows. Except for the low density of linear features in the valleys, little correlation is evident between the density of linear features on the MSS images and lithology (figs. 4 and 2).

The areas of high density of linear features on the SLAR images generally correspond with areas underlain by specific rock types. These include: (1) batholithic rocks in the Pioneer and Highland Mountains, (2) complexly folded and faulted Archean rocks in the cratonic areas of the Ruby Range and southern part of the Tobacco Root Mountains, (3) Tertiary tuffaceous deposits in the Lemhi valley, northern Big Hole River valley, Ruby River valley, and French Creek valley, and (4) Cretaceous-Tertiary volcanic rocks in the south-central part of the quadrangle (figs. 2 and 5). Along the northeastern front of the Beaverhead Mountains, however, the high density of linear features is related primarily to the presence of streams that have cut into morainal deposits. In some areas of batholithic rocks, such as the southeastern Pioneer Mountains and the western slopes of the Beaverhead Mountains and the Bitterroot Range, the lower density of mapped linear features on the SLAR mosaic is caused by the presence of extensive shadows. These same areas have high densities in the MSS linear feature map (fig. 4).

The correspondence between the contour map of the areal density of all linear features (fig. 6) with a map of mines and prospects (Loen and Pearson, 1984) is generally poor. There are many areas where there is a high density of linear features and few known deposits. These results suggest that there is either no spatial correlation between the density of linear features and the distribution of known deposits, or the azimuthal trend and length of the linear features must also be considered.

Length

The length-frequency histogram for linear features on both the MSS and SLAR images is skewed towards longer features. The mode is 0.9 to 1.0 km and the arithmetic mean is 1.62 km. The areal distribution of linear features both greater than or equal to 1 km and less than 1 km show similar patterns; neither corresponds well with lithologic units or the distribution of known deposits. These results suggest that azimuthal trend should be considered to determine if it is more useful for mineral assessment than total areal density or length of linear features.

Azimuthal Trends

A statistical approach was used to determine the azimuthal ranges of significant trends. This approach takes into account the distribution and orientation of the linear features as a method of defining regionally important azimuthal trends which may be related to regional tectonic phenomena. It involves a systematic analysis of the strike-frequency plot of the data. The frequency of observation was weighted according to length of linear features because longer linear features may be important components of the regional tectonic framework. Statistically significant trends were defined by the significance test of Sawatsky and Raines (1981). Linear features of statistically significant trends were plotted and their areal densities were contoured in order to determine locations of lineaments. A 1-km grid cell with a smoothing window of 25 km was used in contouring the data.

The strike-frequency plot for the linear features taken from both Landsat MSS and SLAR images (fig. 7) has a broad high in the northeast direction and a broad low from the northwest to west directions. These trends may be partly related to

enhancement of northeast-trending features and suppression of northwest-trending features due to the northwestward solar illumination of the MSS images. However, northeast-trending linear features are also conspicuous in topographic maps of the quadrangle. Furthermore, northeast trends constitute a broad maximum in the histogram of linear features mapped on the SLAR mosaic (fig. 8), even though features with this orientation were not repeated on the SLAR compilation if they had been mapped on the MSS images. Therefore, we believe that the high frequency of the northeast-trending linear features reflects a prominent topographic, and presumably structural, grain in the quadrangle. Northwest-trending features may be supressed somewhat because of the large shadowed areas in the SLAR mosaic.

Eleven statistically significant maxima were identified in the strike-frequency plot of all linear features (fig. 7). Plots of the linear features constituting these trends show that those linear features belonging to the broad N35°-58°E-trending maximum exhibit local geographic concentrations (fig. 9). The linear features constituting the other significant maxima are distributed more uniformly, although local concentrations are present that indicate the locations of lineaments (see pamphlet appendix). The distributions of N35°-58°E-trending linear features greater than or equal to 1 km and less than 1 km are similar, but the plot of linear features greater than or equal to 1 km facilitated delineation of lineaments and therefore was used throughout the remainder of the analysis.

The contour map of N35°-58°E-trending linear features shows many areas with high density, most of which correspond to batholithic rocks, especially in the Pioneer and Beaverhead Mountains and in the northeastern parts of the quadrangle (figs. 10 and 2). Other areas of high density are coincident with the Archean metamorphic rocks in the southern parts of the Ruby Range and the Tobacco Root Mountains. Cretaceous-Tertiary volcanic rocks in the southeastern, south-central, and southwestern parts of the quadrangle also have a high density of N35°-58°E-trending linear features. Linear features with this orientation are typically much less abundant in the other lithologic units, dominantly sedimentary and metamorphic rocks (figs. 10 and 2). These spatial relationships suggest that the frequency of N35°-58°E-oriented fractures are more abundant in the crystalline terrain. These anomalous areas are of particular interest because they may be indicative of intense fracturing that could be favorable for mineralization. Similarly, non-crystalline areas with an anomalously high density of fractures with this orientation are also of interest. In both types of terrain, some local areas of low density are the result of the presence of glacial deposits.

The high frequency of generally northeast-oriented linear features tends to suppress the relative frequency of northwest-oriented features, and hence the narrowness of the three northwest significant maxima (fig. 7). In order to evaluate the distribution of northwest-oriented linear features further, we plotted the features that constitute each of the five frequency peaks (fig. 7; see pamphlet appendix) which range from north-northwest to west-northwest. The lineaments delineated in these plots are discussed in the next section.

Lineaments

Thirty-five lineaments and two non-linear concentrations of linear features (fig. 11; accompanying map) were identified by visual analysis of the plots of features constituting each of the twelve relative frequency peaks in the histogram (fig. 7). Lineaments were defined in the plots where the pattern of linear features differed from that of surrounding areas or when the relative density of linear features was greater than that of surrounding areas. No lineaments or concentrations were identified in the plot of N9°-10°E-trending linear features. The plots for each relative frequency peak are shown in the pamphlet appendix (figs. A-1 through A-10). Each of the 37 features is also described on the accompanying sheet, along with pertinent geographic, topographic, orientation, geologic, and geophysical data summerized in table format.

Many of the lineaments correspond at least locally to mapped faults, although in a few cases the faults are near the margin of a lineament but not within it. In several cases, lineaments extend beyond the mapped faults for a considerable distance or bridge areas between faults with the same trend, which suggests extensions of these faults. Most of the lineaments also correspond to elongate anomalies or they are perpendicular to gradient directions in the aeromagnetic map (fig. 12) or in the Bouguer gravity anomaly map (fig. 13).

Several lineaments appear to be local expressions of regionally extensive features. L-31 is the longest and widest lineament identified in the quadrangle (fig. 11 and accompanying map). It extends about 90 km west-northwest from near Sugarloaf Mountain in the eastern Pioneer Mountains to the central part of the Beaverhead Mountains; the average width is approximately 10 km. In the Pioneer Mountains, several faults with this orientation have been mapped within the lineament, but none have been mapped along it in the Beaverhead Mountains. However, there is a marked change in the topography and the distribution of glacial and fluvial deposits along the eastern front of the Beaverhead Mountains where the lineament occurs. Southwest of Johnson Creek, stream valleys are narrow and glacial deposits are restricted, whereas between Johnson and Hell Roaring Creeks, which are near the boundaries of L-31, stream valleys are broad and glacial deposits are more extensive within a recess in the range front. In addition, this area corresponds with an aeromagnetic low which has the same dimensions and west-northwest orientation. This low extends across the Big Hole valley to the eastern front of the Pioneer Mountains, although it is punctuated locally by isolated high and low anomalies. Therefore, we believe that L-31 marks an important structural zone in the quadrangle.

L-14 and L-24 are related to linear segments of the Beaverhead River in the mountain range in the south-central part of the quandrangle and in the valley northeast of Dillon, Montana, respectively. Faults have been mapped within L-24 and at the southwest terminus of L-14. Although no faults have been mapped in the area between these two lineaments, we believe that faults may be present here. Mapped faults are also present north-northwest of L-24. These faults may extend from the south-central margin of the quadrangle northeastward along the Beaverhead River valley and north-northeastward along the

Jefferson River valley to the northeast quadrangle boundary. Ruppel (1982) shows a lineament with similar orientation and extent located about 15 km to the northwest in the south-central part of the quadrangle.

L-13, L-11, and L-20 do not appear to be continuous with one another at a scale of 1:250,000. There are gaps in the linear features patterns between them. This is especially apparent where the Big Hole basin passes between L-13, which lies to the south, and L-11, which lies to the north. However, when viewed on the MSS band 7 mosaic prepared by the U.S. Soil Conservation Service at a scale of 1:2,500,000, these features appear to be quite continuous and to extend northeastward 120 km into the White Sulphur Springs, Montana 1° X 2° quadrangle to Ringing, Montana, and possibly 45 km further to just south of Martinsdale Reservoir and Gordon Butte. The extension of the feature in the southwestern direction into the Challis, Idaho 1° X 2° quadrangle is not as clear.

According to our interpretation of regional structural and stratigraphic data by O'Neill and Lopez (1985), L-8 and L-9 are elements of the Great Falls tectonic zone that extends northeastward from the Idaho batholith into southwestern Saskatchewan, Canada (fig. 14). L-9 is coincident with a zone of northeast-trending faults, whereas L-8 represents topographic lows along faults and highs where granitic dikes were emplaced along some of these faults (Elliott and others, 1986). Related faults are present where the zone continues southwestward to Salmon, Idaho. Recurrent movement from middle Proterozoic to Holocene time influenced the thickness of sedimentary rocks and orientation and localization of intrusive rocks and related metal deposits (O'Neill and Lopez, 1985).

Southeast of L-8 and L-9 along the range front, L-3 appears to be related to a series of faults that comprise the Anaconda fault (fig. 14) (O'Neill and Lopez, 1985). The Anaconda fault is interpreted as the northeastward continuation of the Shoup and Hot Springs faults which form a continuous zone 120 km to the southwest of L-3. Late Tertiary and Quaternary movements have been inferred along this fault (O'Neill and Lopez, 1985). The abrupt change of the L-3 trend from northeast to northwest is conspicuous on Landsat MSS images. Although northwest-trending faults have not been mapped along the segment of L-3 with this trend, which is located in Quaternary glacial and valley-fill deposits (Ruppel and others, 1983), major northwest-trending faults cut the Big Hole valley about 5 km to the south. In addition, this segment of the lineament is located about 2 km southwest of the apparent termination of the McCartney Mountain fault, a major northwest-oriented fault (Ruppel, 1982; Ruppel and others, 1983). West-northwest-oriented aeromagnetic anomalies are coincident with this part of L-3.

L-22 may be related to a major fault located to the southwest (fig. 14). The Panther Creek fault trends $N33^{\circ}$-$38^{\circ}E$ for about 55 km west of the quadrangle boundary. Although L-22 trends about $N45^{\circ}E$, it is composed of linear features that trend $N35^{\circ}$-$58^{\circ}E$, $N61^{\circ}$-$65^{\circ}E$, and $N30^{\circ}$-$31^{\circ}E$. The presence of several northeast-oriented linear features northeast of L-22 and terminations in aeromagnetic trends in this area may suggest that the structural zone is broader and extends further to the northeast than L-22 indicates.

Arcuate Features

The majority of the the arcuate features that were identified on the SLAR and MSS images were interpreted to be related to glaciation. These will not be discussed because they are not pertinent to the task of mineral assessment. Two arcuate features mapped on MSS and SLAR images were interpreted to be unrelated to glaciation (fig. 11 and accompanying map).

Arcuate feature A encompasses the western half of McCartney Mountain, which is a Cretaceous granodiorite intrusive body. The northern margin of the arc follows a creek which is coincident with the boundary between the intrusive body and the Cretaceous Colorado Group to the north. The feature lies within and is concentric to a larger circular high in the aeromagnetic data (fig. 12) which corresponds to the intrusive. There is no good correspondence between this arcuate feature and the gravity data (fig. 13).

Arcuate feature B is a small ellipse that lies north of Grasshopper Creek. It marks the outline of a small volcanic center (B.R. Berger, USGS, oral commun., 1984) and lies in a saddle between two highs in the aeromagnetic data (fig. 12). Again, there is no good correspondence between this feature and the gravity data (fig. 13).

Composite Map

As a final stage of the analysis, data from the lineament and arcuate feature map (fig. 11), contour map of $N35^{\circ}$-$58^{\circ}E$-trending linear features (fig. 10), and the map of hydrothermally altered rocks (fig. 15) were combined. This was accomplished by gridding each data set into 5 km X 5 km grid cells. The cells were assigned values dependent upon the presence or absence of the characteristic features of each data set. The values were chosen on the basis of their relative importance to an analysis of mineral potential (table 1).

The presence of hydrothermally altered rocks within a cell was considered to be the most valuable feature, because in most hydrothermal ore deposits, some wall-rock alteration is associated with metal deposition. The distribution of $N35^{\circ}$-$58^{\circ}E$-trending linear features with lengths of 1 km or greater was considered to be second in importance because of their value as an indicator of fracturing, especially in crystalline rocks. The lineaments and arcuate features were considered the least important; however they may represent faulting, fracturing, and crustal weakness which can be important to the localization of metal deposits.

A composite grid was produced by adding the values of corresponding cells of the three gridded data sets, and these results were contoured (fig. 16). Higher contour values indicate areas of greater mineral potential. Because both the gridded lineament and $N35^{\circ}$-$58^{\circ}E$-trending linear features data sets were derived from the plot of all of the linear features (accompanying map) there is duplication of data in some of the grid cells where lineaments were defined using linear features whose trends range from $N35^{\circ}$-$58^{\circ}E$. In these situations a value of 4, which corresponds to the value given to a cell containing $N35^{\circ}$-$58^{\circ}E$-trending linear features, was assigned to the grid cell, rather than a composite value of 6 which

would result from adding the assigned lineament value to the N35°-58°E-trending linear features value.

Interpretation

The composite map (fig. 16) shows a cluster of high values in the Pioneer Mountains and several isolated highs in the other mountain ranges. As expected, low values occur mainly in the basins. In the Pioneer Mountains, the high values form a northwest-oriented belt extending for about 45 km from near Torrey Mountain in the southeast to the northwestern margin of the range. The belt may extend for another 17 km southeast of Torrey Mountain, but the presence of the large area of Quaternary glacial deposits interrupts its continuity in this area. The belt is located along the southwestern margin of the major northwest-oriented lineament (L-31, fig. 11 and accompanying map) because of the strong influence of several hydrothermally altered areas (Segal and Rowan, 1989). Subordinate trends in the Pioneer Mountains are northeast and, at the western margin, west (fig. 16).

Broad northeast-trending areas with moderately high composite values are present in the southwestern and northeastern parts of the quadrangle (fig. 16). High values within these broad areas are related mainly to the presence of hydrothermally altered areas and, in some areas, to the intersection of lineaments coupled with a high density of N35°-58°E-trending linear features. As previously mentioned, we believe that the northeast-oriented areas in the southwestern and northeastern parts of the quadrangle are aligned with northeast trends in the southern and eastern Pioneer Mountains and constitute a major structural zone that may continue northeast of the Dillon quadrangle.

The northeast trends in the northwestern part of the quadrangle interpreted to be elements of the Great Falls structural zone (O'Neill and Lopez, 1985) are obscured somewhat in the composite map by the presence of several lineaments with trends other than northeast (fig. 11) and concentrations of N35°-58°E-trending linear features that do not constitute lineaments (fig. 10). However, the proposed northeast extension of the Panther Creek fault, a part of which is represented by L-22 (fig. 14), is evident in the composite map (fig. 16).

Moderately high to high composite values are widespread in the Tobacco Root Mountains and Ruby Range (fig. 16). In the southern part of the Ruby Range, northwest- and northeast-trending contour gradients are conspicuous, owing to the high density of linear features with these orientations.

In order to evaluate the usefulness of the composite map for mineral assessment we compared it with a contour map of mines and prospects in the quadrangle (fig. 17). The contour map was prepared by determining the percentage of mines and prospects located within each 5 km X 5 km grid cell and contouring the results. All the mines (Loen and Pearson, 1984) were contoured except those located in coal, bentonite, stone, clay, onyx, and phosphate deposits. These deposits were excluded because their occurrence is probably not directly controlled by fracturing and typically hydrothermally altered rocks are not present. Placer gold deposits are considered separately. In preparing the contour map, the value of commodities produced was not considered.

Use of the contour map of mines and prospects for determining the merits of the composite map assumes that the deposits considered are characterized by the factors expressed in the composite map. The validity of this assumption can be tested by examining the overall correspondence between the patterns shown in the maps. Good correspondence would indicate that the assumption is reasonable, and high values in the composite map that do not correspond to the locations of mines and prospects should be noted as promising, unexplored areas. Disagreements between the two map patterns in which there is a high value in the contour map of mines and prospects and a low value in the composite map might have several explanations, including the presence of shadows that would mask linear features on the MSS and SLAR images and the lack of alteration in association with known deposits.

In the eastern three-fourths of the quadrangle, the agreement between the composite map and contour map of mines and prospects is good (figs. 16 and 17, respectively). The correspondence of the map patterns in the Pioneer Mountains is particularly striking. Several differences, however, are notable. The area of high values in the composite map located near longitude 113°02' W, latitude 45°43' N may be an area of high potential that has not been explored systematically (fig. 16, area A). A high density of N35°-58°E-trending linear features form a crude circular pattern in this area (fig. 10), and a small area of hydrothermally altered rocks is present (fig. 15). Another promising area with few mines and prospects is located about 14 km to the south-southwest of the Hecla district (fig. 16, area B). N35°-58°E-trending linear features are concentrated here, and several areas of hydrothermally altered rocks are exposed.

The composite map values suggest that the area of high values forming the northwest-trending belt across the Pioneer Mountains (fig. 16) may be more important than the contour map of mines and prospects (fig. 17) indicates. Although the patterns here are very similar in the two maps, only a few mines and prospects are shown by Loen and Pearson (1984) and the composite values are very high, especially in the northwestern part (fig. 16). Also, no mines and prospects are shown along the belt that extends northeastward from the southeastern terminus of this belt (fig. 17).

In the southwestern Pioneer Mountains, moderately high composite map values are present in a fairly large area that is centered near longitude 113°19' W, latitude 45°28' N (fig. 16, area C), but only a few mines and prospects are present (fig. 17). As D.B. Segal (USGS, oral commun., 1983) pointed out, the Deer Peak area, consisting of limonitic quartzite situated within this area, may deserve detailed examination because a geochemical anomaly has been detected here (B.R. Berger, USGS, oral commun., 1983). The area with high values located approximately 12 km southeast of this area is also of interest, although the pair of 6-level contoured areas are due to splitting of a moderately large altered area between two grid cells rather than being indicative of two distinct promising areas (fig. 16, area D).

One area in the Pioneer Mountains stands out in the comparison of figures 16 (area E) and 17 because a density of mines and prospects is not coincident with high value in the composite map. This area is located about 10 km east-southeast of longitude 113°00' W,

latitude 45°45' N in the northern part of the Quartz Hill mining district (Loen and Pearson, 1984). A large part of this area is covered by Quaternary glacial deposits and the remainder consists mainly of Paleozoic sedimentary rocks (Ruppel and others, 1983), in which limonitic hydrothermal alteration typically is limited in areal extent.

In the northeastern part of the quadrangle, correspondence between the figure 16 and figure 17 map patterns is generally good, including the presence of north-trending highs within broad northeast-oriented moderately high areas. The most conspicuous area with a high areal density of mines and moderately low composite map values is located near longitude 112°25' W, latitude 45°52' N in the Homestake mining district (Loen and Pearson, 1984) (fig. 16, area F; fig. 17). This area consists of Cretaceous batholithic rocks, and the dominant metal deposits are silver, gold, copper, lead, and placer deposits. The density of linear features in this area is relatively low, but two areas of limonitic rocks near the southwestern margin have not been examined in the field to determine if hydrothermally altered rocks are present (D.B. Segal, USGS, oral commun., 1983).

Two similar discrepancies occur near longitude 112°36' W, latitude 45°30' N (fig. 16, area G; fig. 17). The northernmost area is the McCartney Mountain district where silver, lead, gold, and molybdenum are associated with Cretaceous intrusive rocks (Loen and Pearson, 1984). Although a conspicuous arcuate feature was mapped here (fig. 11), the lack of other elements comprising the composite map resulted in the moderately low values in figure 16. The area shown to the south in the contour map of mines and prospects (fig. 17) that corresponds to area H in figure 16 marks two manganese mines in Paleozoic sedimentary rocks (Loen and Pearson, 1984; Ruppel and others, 1983).

The generally good agreement between the composite map and the contour map of mines and prospects in the southeastern part of the quadrangle is somewhat surprising, because the deposits shown in figure 17 are a combination of talc and manganese, which are probably metasedimentary in origin. Small occurrences of graphite and copper appear to be controlled at least partly by fractures (Heinrich, 1960; Loen and Pearson, 1984). The high composite map values in the southern part of the Ruby Mountains reflect the presence of numerous N35°-58°E-trending linear features (fig. 10) and two northwest-oriented lineaments (L-35 and L-36, fig. 11 and accompanying map). The northwest-oriented lineaments are expressions of faults and dikes with which some of the copper deposits are associated (Heinrich, 1960). The two highest composite values in this region (fig. 16) are related to the presence of hydrothermally altered rocks (Segal and Rowan, 1989), as well as high density of N35°-58°E-trending linear features (fig. 10). Although some of these linear features may reflect lithologic layering, we believe that many are probably the expression of fractures.

Agreement between the composite map and the mines and prospects contour map is poorest in the western one-fourth of the quadrangle (figs. 16 and 17, respectively). In the northwestern part, the broad arcuate band of moderately high values in the composite map is the product of several northwest- and northeast-oriented lineaments (fig. 11) and numerous northeast-trending linear features. However, the northeast-oriented linear features and lineaments are locally related to granitic dikes that have some associated mineralization (J.M. O'Neill, USGS, oral commun., 1983). Therefore, parts of this arcuate zone may have some potential for metal deposits.

The Gibbonsville mining district (Loen and Pearson, 1984) located near the west-central margin of the quadrangle is not indicated by corresponding high composite map values, except in the eastern part (figs. 16 and 17). In the vicinity of Granite Mountain, where the highest areal density of mines occurs (fig. 16, area I), the overall density of linear features is relatively low in MSS images (fig. 4). Although numerous linear features are suggested in the SLAR images, shadows made precise delineation of the features difficult. Apparently, any features manifested as linear features here are too small to be detected in MSS images, and multiple illumination directions would be needed to map them in radar images.

South of the Gibbonsville district near longitude 113°56' W, latitude 45°16' N, composite values are also low where the areal density of mines is relatively high in the Eureka district (fig. 16, area J; fig. 17, respectively). Few linear features are evident here in the MSS images (fig. 4), but a moderately large number of N35°-58°E-trending linear features were delineated in the SLAR mosaic (fig. 5). However, the lack of altered areas, lineaments, and arcuate features resulted in moderately low composite values.

Placer Gold Deposits

Placer gold deposits were examined separately (fig. 18), because the horizontal extent of many of these deposits make their inclusion in the mines and prospects contour map difficult. Comparison of the distribution of placer deposits with the composite map shows that most of the deposits occur within areas of moderately high to high composite values (figs. 18 and 16). This result is not surprising because of the good agreement between the composite map and mines and prospects contour map (figs. 16 and 17) and the genetic relationship between placers and nearby in situ gold deposits. The main exceptions to this generally good agreement are in the western and northern part of the Gibbonsville and Homestake mining districts and in the southeastern part of the quadrangle (figs. 16 and 18). At least part of the explanation for the lack of agreement in the southeastern part of the quadrangle is that the placer deposits are located in a part of the quadrangle where hydrothermally altered rocks have not been mapped (Segal and Rowan, 1989).

SUMMARY

Thirty-five lineaments, two non-linear concentrations of linear features, and two arcuate features were derived from Landsat MSS and SLAR images and mapped on the Dillon 1° X 2° quadrangle, Montana and Idaho. Most of the lineaments have some mapped faults associated with them, and several of the lineaments are associated with large zones of faulting or shearing. In some instances extensions of mapped fault systems can be inferred. Many of the lineaments correspond to anomalies or are parallel to gradient directions in the aeromagnetic or gravity data. Those lineaments that do not follow the trends of any mapped structures but are expressed in the aeromagnetic and gravity data may represent

discontinuities at depth which are manifested as zones of fracturing at the surface.

Several regionally extensive lineaments were identified during the analysis (fig. 11). L-31 is a northwest-trending zone which extends across the Pioneer Mountains and the Big Hole River valley to the Beaverhead Mountains. L-13, L-11, and L-20 appear to be related to a very extensive northeast-trending feature that cuts through the quadrangle. L-14 and L-24 correspond to several mapped faults and may be segments of a more continuous fault system. L-8 and L-9 have been interpreted as being components of the Great Falls tectonic zone. L-22 is a northeast-trending feature that has been inferred to be the continuation of the Panther Creek fault zone which lies to the southwest.

The statistical method used in this analysis identified the N35°-58°E-trending linear features as being statistically significant. The contour map of the N35°-58°E-trending features that are 1 km or longer shows a good correspondence to the generalized geologic map. The areas of high density on the contour map are generally coincident with intrusive rocks and Cretaceous-Tertiary volcanic rocks. The areas of low density are associated with sedimentary rocks. Metamorphic rocks do not have a unique signature on the contour map of N35°-58°E-trending features. This relationship is valuable because it highlights batholithic rocks with intense fracturing.

The information derived from the analyses of linear features and arcuate features was combined with data from a map of hydrothermally altered rocks. The resulting composite map can be utilized in the assessment of the mineral potential in the Dillon 1° X 2° quadrangle. Comparison of the composite map with a contour map of the mines and prospects in the quadrangle indicates several areas which have high values in the composite map and low values in the contour map of mines and prospects. The areas that stand out most in this approach lie in the Pioneer Mountains. The two most significant areas occur south of the Big Hole River around longitude 113°02' W, latitude 45°43' N and 14 km south-southwest of the Hecla mining district. There is an area of moderately high values in the vicinity of Deer Peak in the southwestern Pioneer Mountains that should be considered further. The northwest-trending belt in the Pioneer Mountains shows up in the contour map of mines and prospects; however it appears to be more significant in the composite map. These areas have been indicated as meriting further investigation.

REFERENCES

Elliot, J.E., Wallace, C.A., O'Neill, J.M., Hanna, W.F., Rowan, L.C., Segal, D.B., Zimbelman, D.R., Pearson, R.C., Close, T.J., Federspiel, F.E., Causey, J.D., Willett, S.L., Morris, R.W., and Huffsmith, J.R., 1985, Mineral resource potential map of the Anaconda-Pintlar Wilderness and contiguous roadless area, Granite, Deer Lodge, Beaverhead, and Ravalli Counties, Montana: U.S. Geological Survey Miscellaneous Field Studies Map MF-1633-A, scale 1:50,000.

Hassimer, J.H., Kaufmann, H.E., and Hanna, W.F., 1986, Description of magnetic tape containing the principle facts for gravity stations in and adjacent to the Dillon 1° X 2° quadrangle, Montana and Idaho: NTIS report PB86-197407/AS.

Heinrich, E.M., 1960, Geology of the Ruby Mountains and nearby areas in southwestern Montana: Montana Bureau of Mines and Geology Memoir 38, part 2, p. 15-40.

Kaufmann, H.E., Sorensen, S.B., and O'Neill, K.J., 1983, Principal facts and complete Bouguer gravity anomaly map for the Dillon 1° by 2° quadrangle, Montana and Idaho: U.S. Geological Survey Open-File Report 83-51, 76 p.

Loen, J.S. and Pearson, R.C., 1984, Mines and prospects of the Dillon 1° X 2° quadrangle, Idaho and Montana: U.S. Geological Survey Open-File Report 84-377, 93 p.

O'Leary, D.W., Friedman, J.D., and Pohn, H.A., 1976, Lineament, linear, lineation; some proposed new standards: Geological Society of America Bulletin, v. 87, p. 1463-1469.

O'Neill, J.M. and Lopez, D.A., 1985, Character and regional significance of the Great Falls tectonic zone of east-central Idaho and west-central Montana: American Association of Petroleum Geologists Bulletin v. 69, no 3, p. 437-447.

Reynolds, M.W., 1979, Character and extent of basin-range faulting, western Montana and east-central Idaho: Rocky Mountain Association of Geologists, Utah Geological Association Basin and Range Symposium, p. 185-193.

Rowan, L.C. and Purdy, T.L., 1985, Analysis of linear features in the Wallace 1° X 2° quadrangle, Idaho-Montana: U.S. Geological Survey Miscellaneous Field Studies Map MF-1354-H, scale 1:250,000.

Ruppel, E.T., 1982, Cenozoic block uplifts in east-central Idaho and southwest Montana: U.S. Geological Survey Professional Paper 1224, 24 p.

Ruppel, E.T., O'Neill, J.M., and Lopez, D.A., 1983, Preliminary geologic map of the Dillon 1° X 2° quadrangle, Montana-Idaho: U.S. Geological Survey Open-File Report 83-168, scale 1:250,000.

Ruppel, E.T., Wallace, C.A., Schmidt, R.G., and Lopez, D.A., 1981, Preliminary interpretation of the thrust belt in southwest and west-central Montana and east-central Idaho: Montana Geological Society Field Conference and Symposium Guidebook to Southwest Montana, p. 139-159.

Sawatsky, D.L. and Raines, G.L., 1981, Geologic uses of linear features maps derived from small-scale images, *in* Proceedings of the Third International Conference on Basement Tectonics, Durango, Colorado, May 15-19, 1978, Basement Tectonics Committee , Inc., p. 91-100.

Segal, D.B. and Rowan, L.C., 1989, Map showing exposures of limonitic rocks and hydrothermally altered rocks in the Dillon 1° X 2° quadrangle, Idaho and Montana: U.S. Geological Survey Miscellaneous Investigations Series Map I-1803-A, scale 1:250,000.

APPENDIX

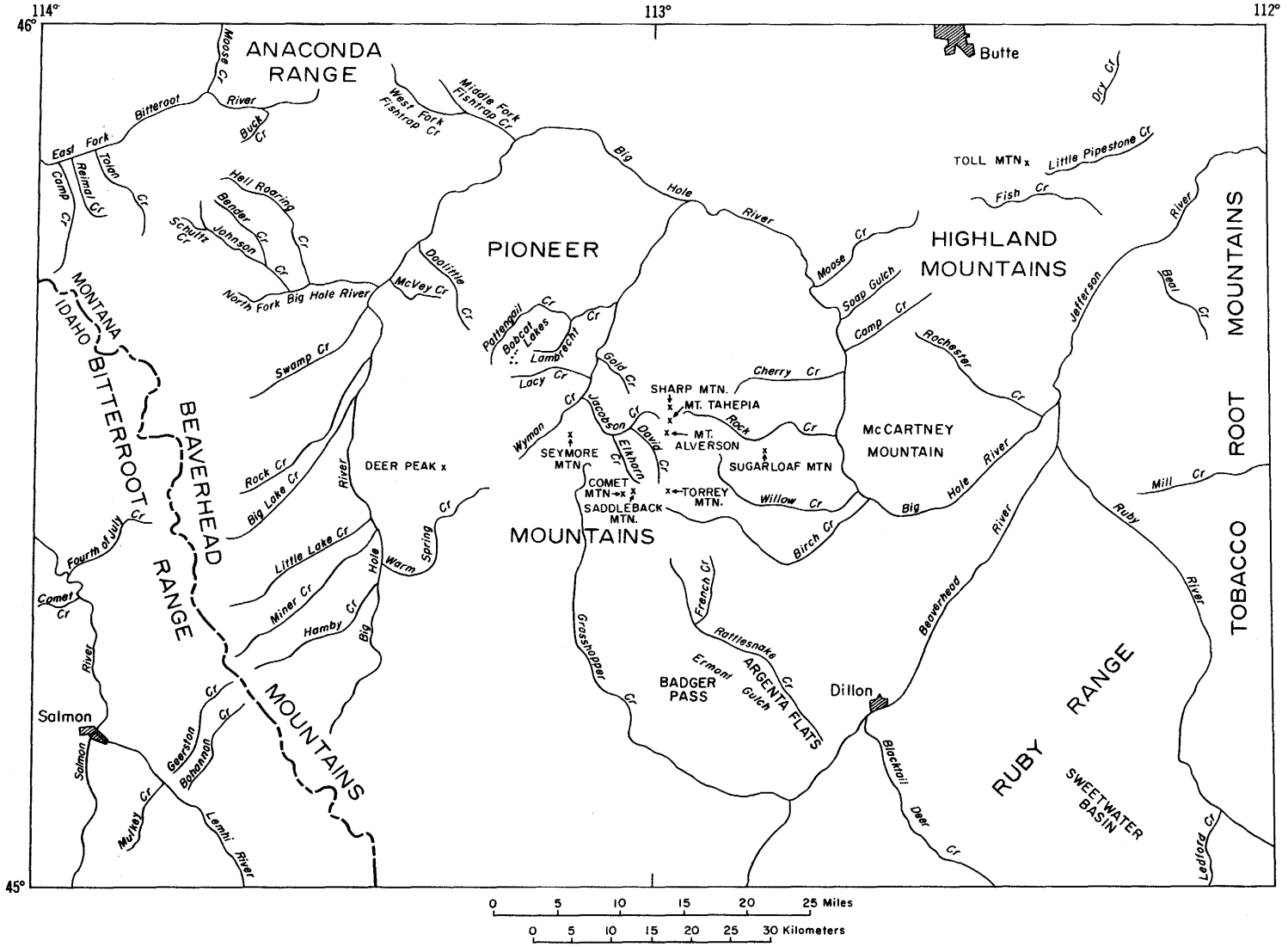

Figure 1.—Selected topographic, physiographic, hydrologic, and cultural features in the Dillon 1° × 2° quadrangle, Idaho and Montana.

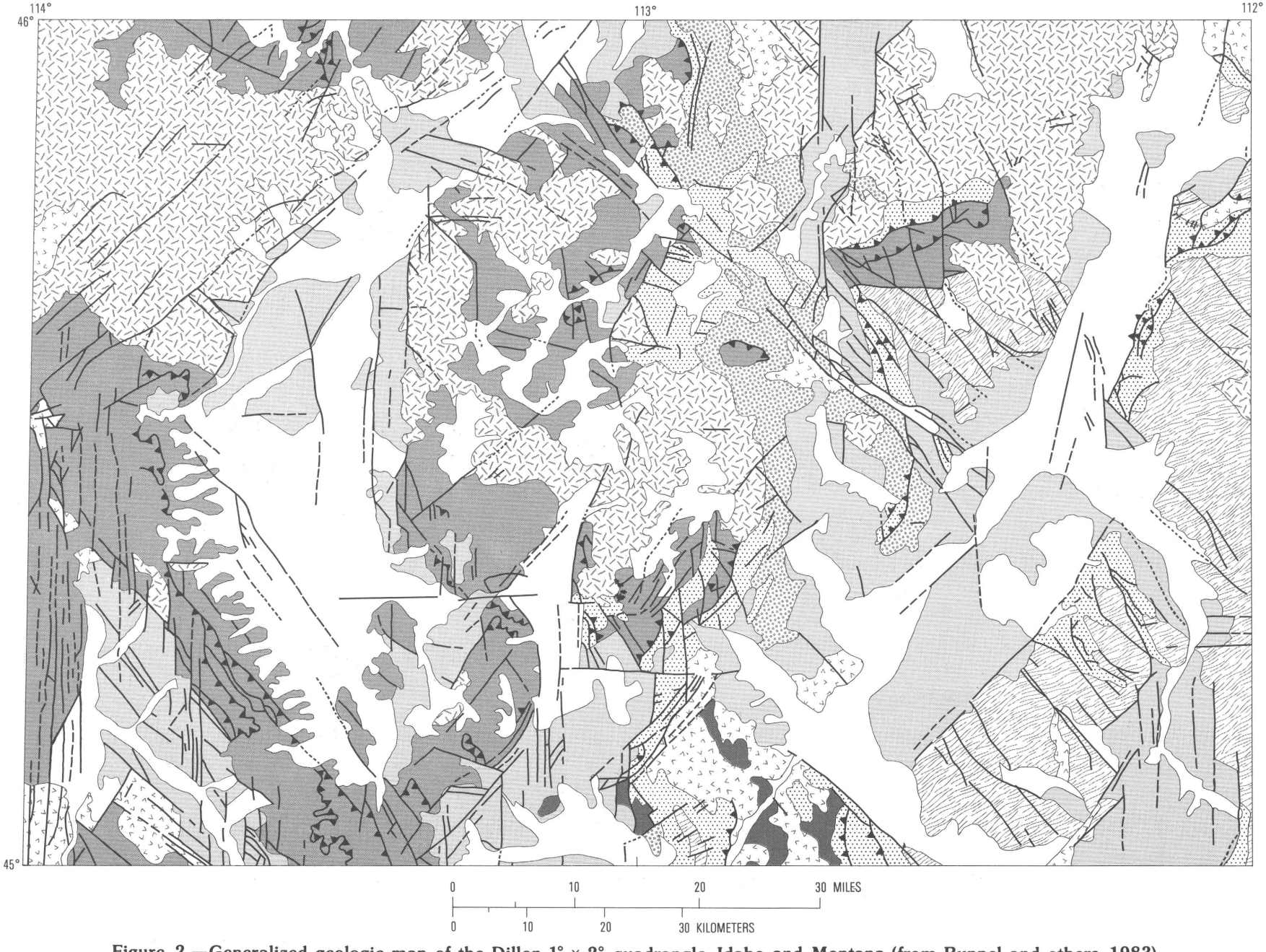

Figure 2.—Generalized geologic map of the Dillon 1° × 2° quadrangle, Idaho and Montana (from Ruppel and others, 1983).

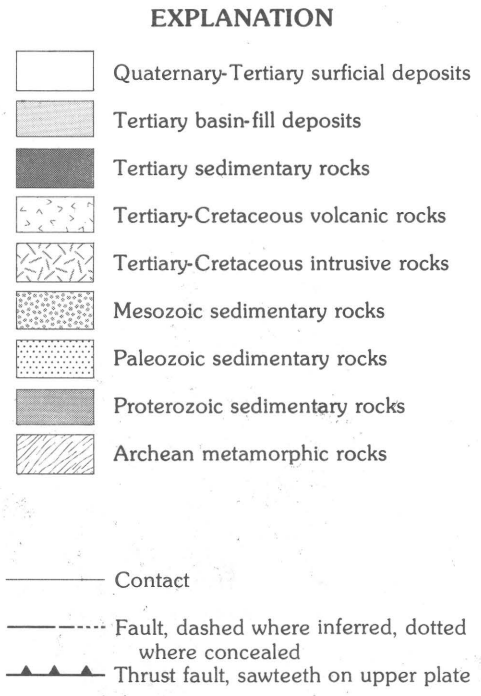
EXPLANATION
Quaternary-Tertiary surficial deposits
Tertiary basin-fill deposits
Tertiary sedimentary rocks
Tertiary-Cretaceous volcanic rocks
Tertiary-Cretaceous intrusive rocks
Mesozoic sedimentary rocks
Paleozoic sedimentary rocks
Proterozoic sedimentary rocks
Archean metamorphic rocks
Contact
Fault, dashed where inferred, dotted where concealed
Thrust fault, sawteeth on upper plate

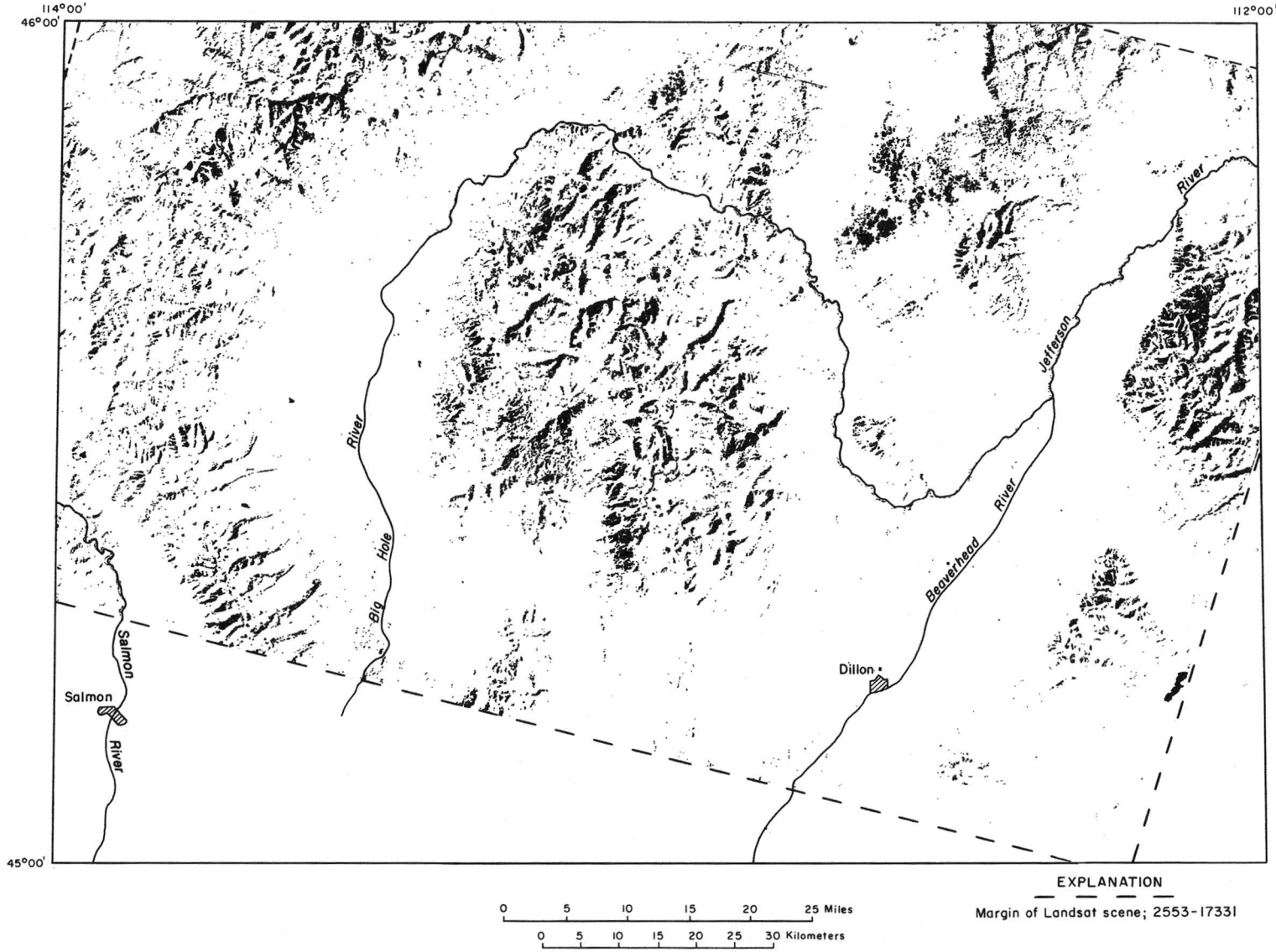

Figure 3.—Shadowed areas in Landsat multispectral scanner (MSS) image 2553–17331, acquired July 28, 1976.

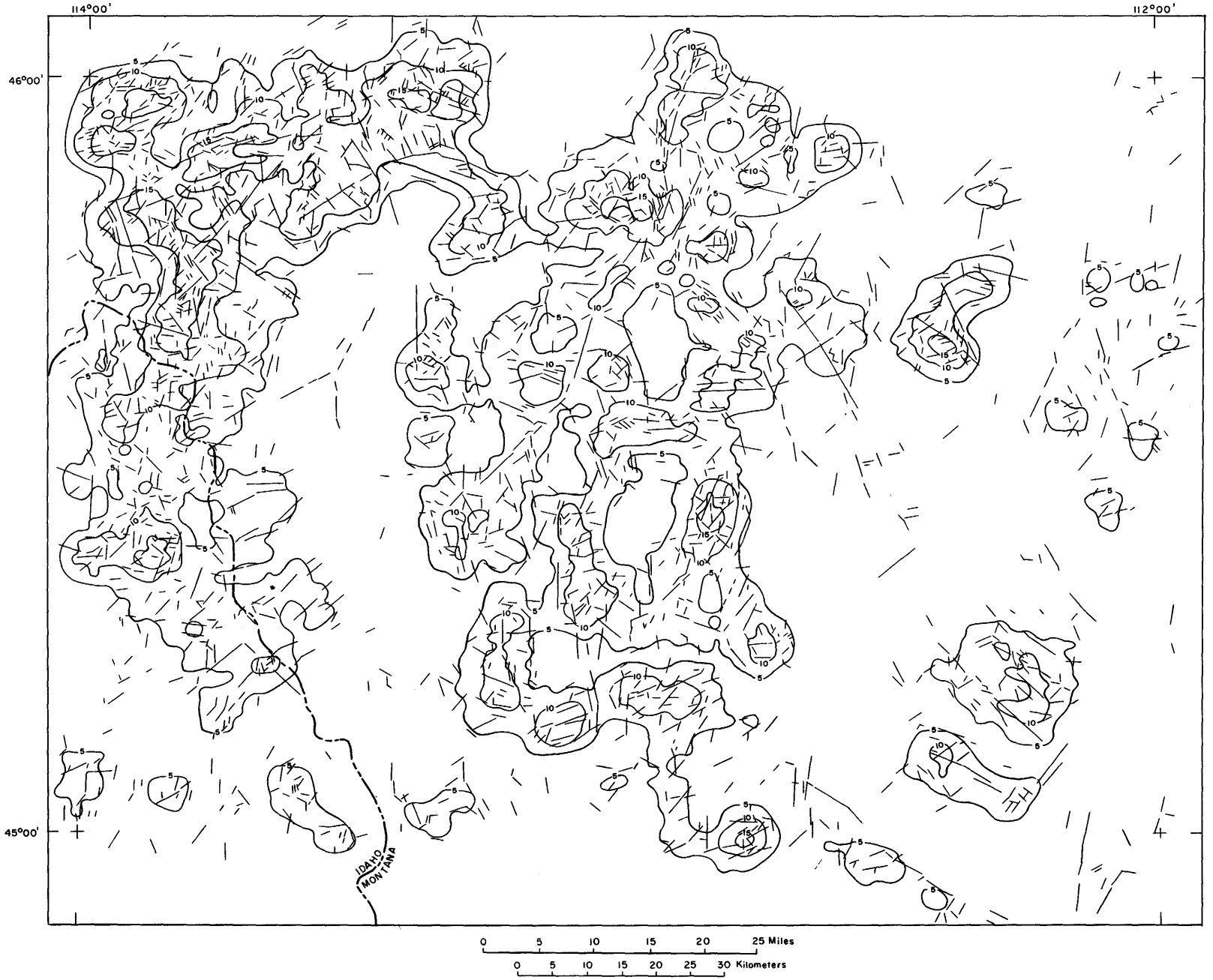

Figure 4.—Contour map showing the areal density of linear features mapped on the Landsat scanner (MSS) images for the 1° × 2° quadrangle, Idaho and Montana.

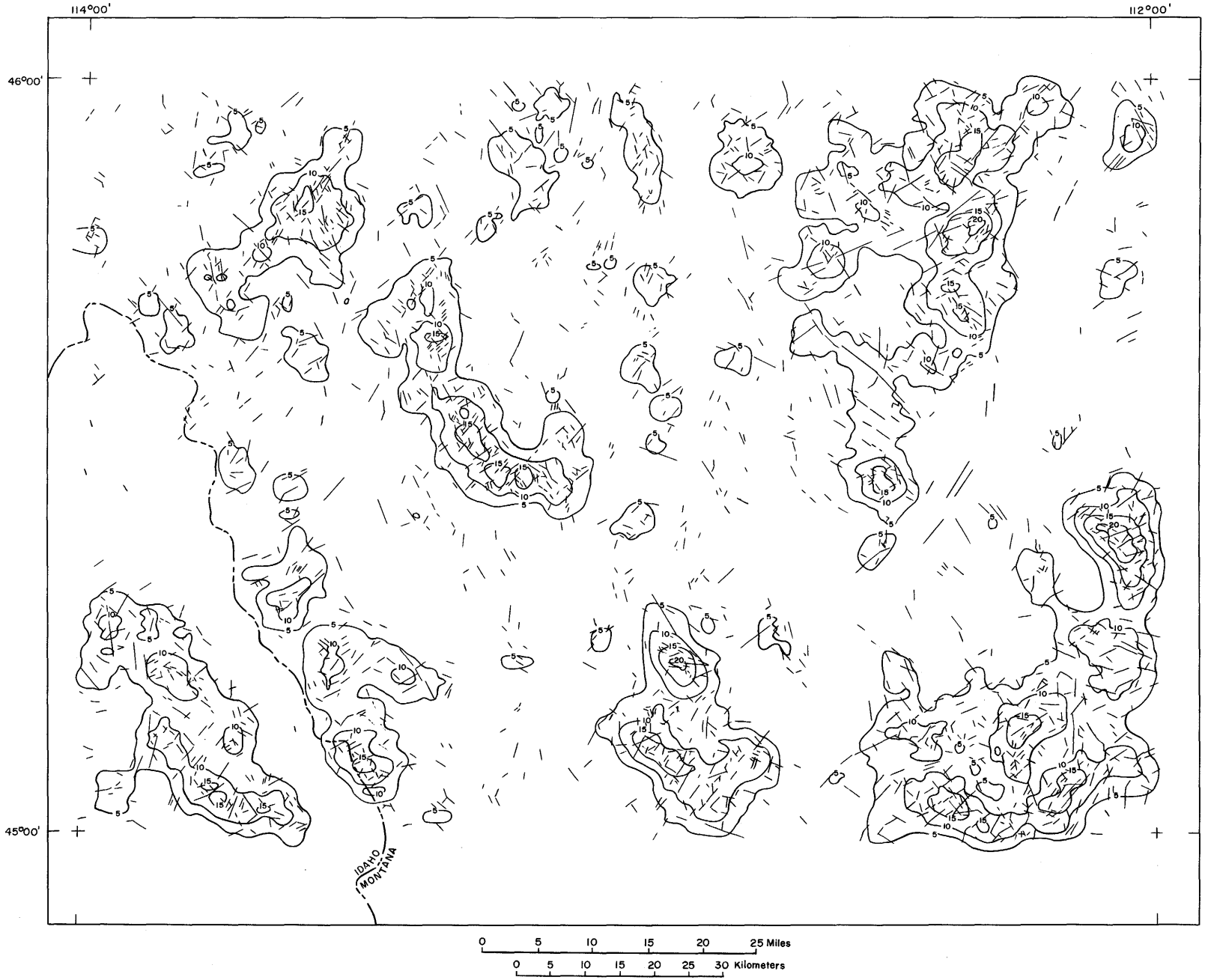

Figure 5.—Contour map showing the areal density of linear features mapped from a side-looking airborne radar (SLAR) mosaic for the Dillon 1° × 2° quadrangle, Idaho and Montana.

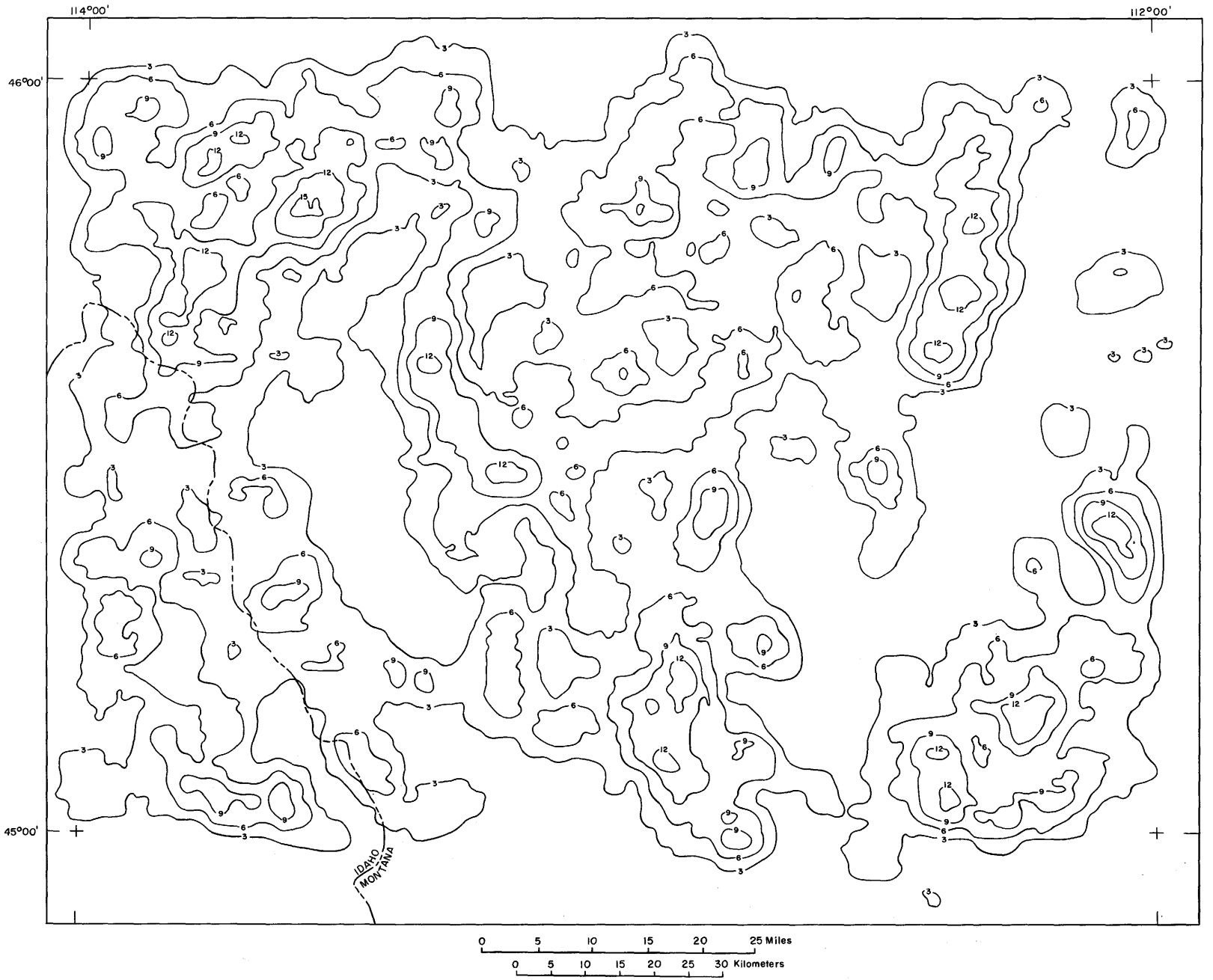

Figure 6.—Contour map showing the areal density of linear features mapped on Landsat multispectral scanner (MSS) and side-looking airborne radar (SLAR) images of the Dillon 1° × 2° quadrangle, Idaho and Montana.

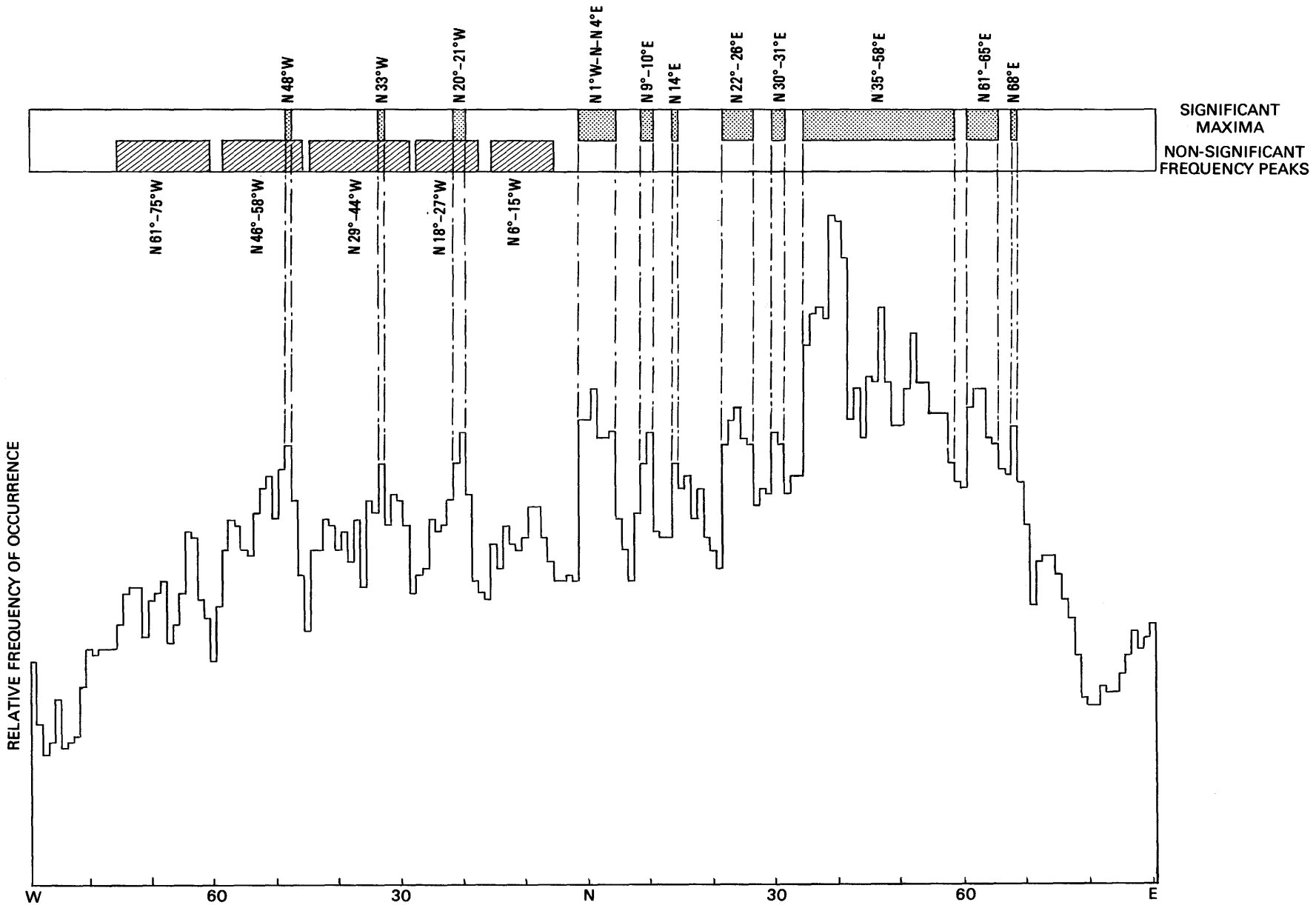

Figure 7.—Length-weighted, strike-frequency histogram for linear features mapped on Landsat multispectral scanner (MSS) and side-looking airborne radar (SLAR) images. Significant maxima and non-significant relative frequency peaks are shown.

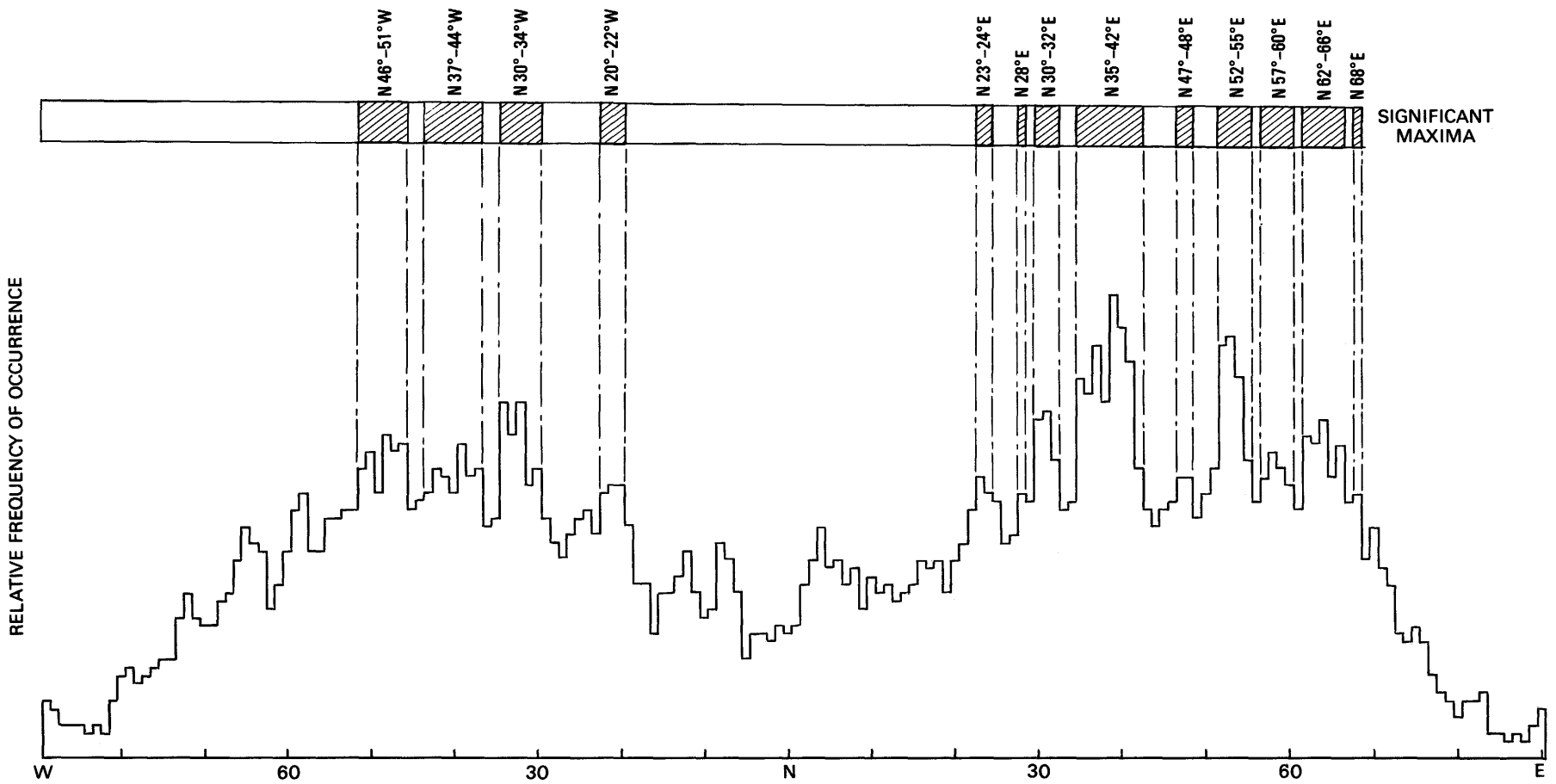

Figure 8.—Length-weighted, strike-frequency histogram for linear features mapped on the side-looking airborne radar (SLAR) mosaic.

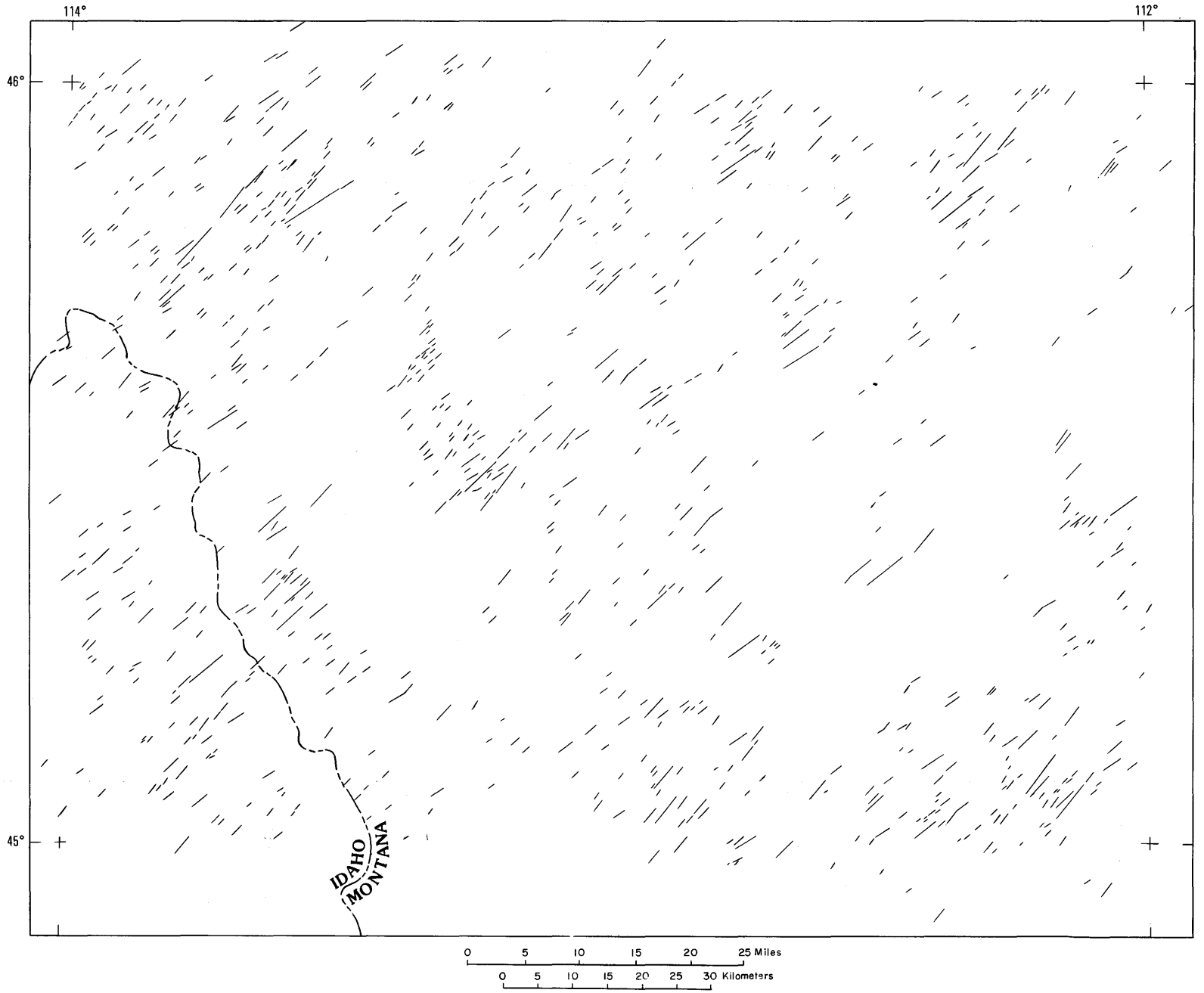

Figure 9.—Map showing N35°–58°E–trending linear features mapped from Landsat multispectral scanner (MSS) and side-looking airborne radar (SLAR) images in the Dillon 1° × 2° quadrangle, Idaho and Montana.

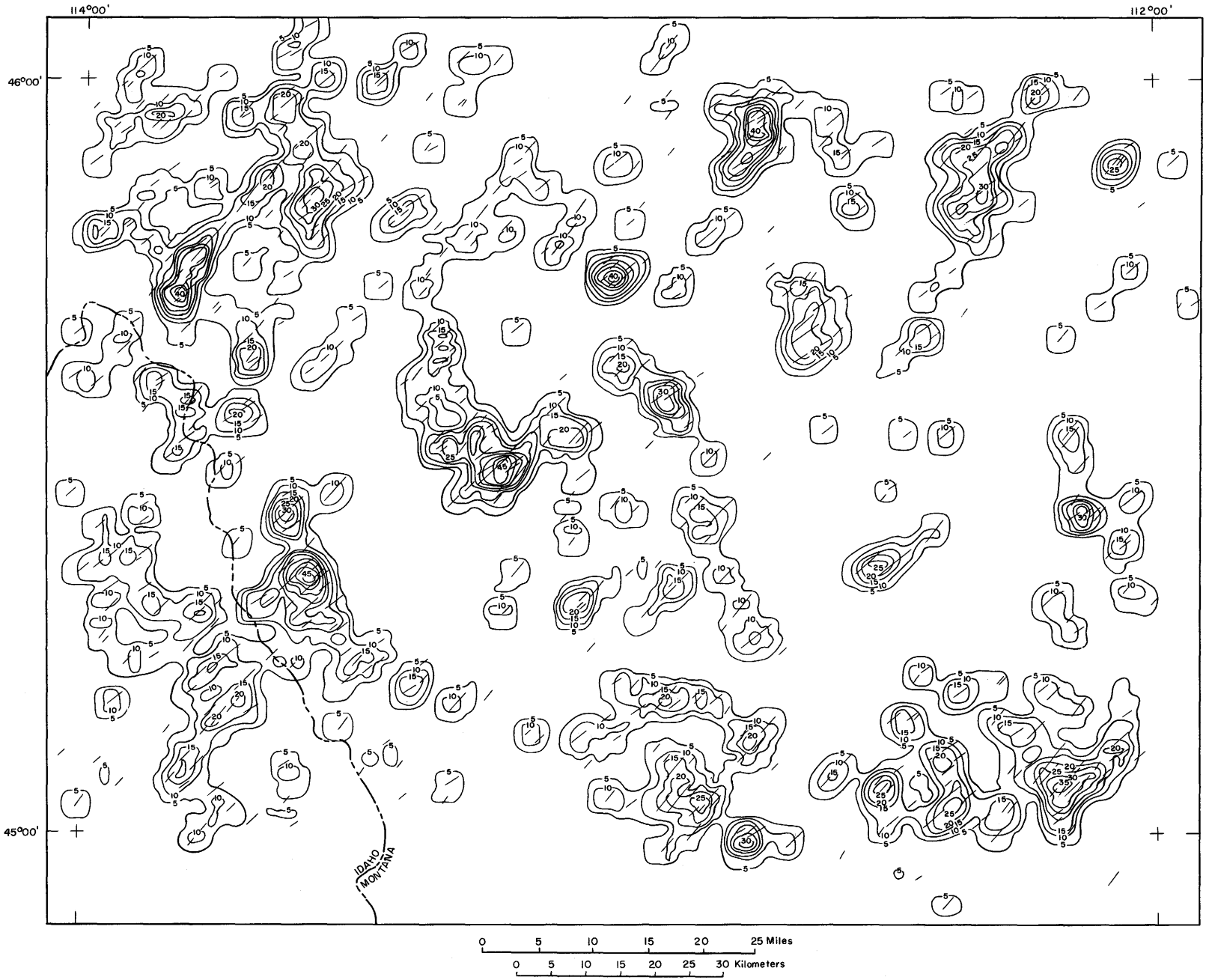

Figure 10.—Contour map showing the areal density of N35°–58°E–trending linear features 1 km and longer from Landsat multispectral scanner (MSS) and side-looking airborne radar (SLAR) images in the Dillon 1° × 2° quadrangle, Idaho and Montana.

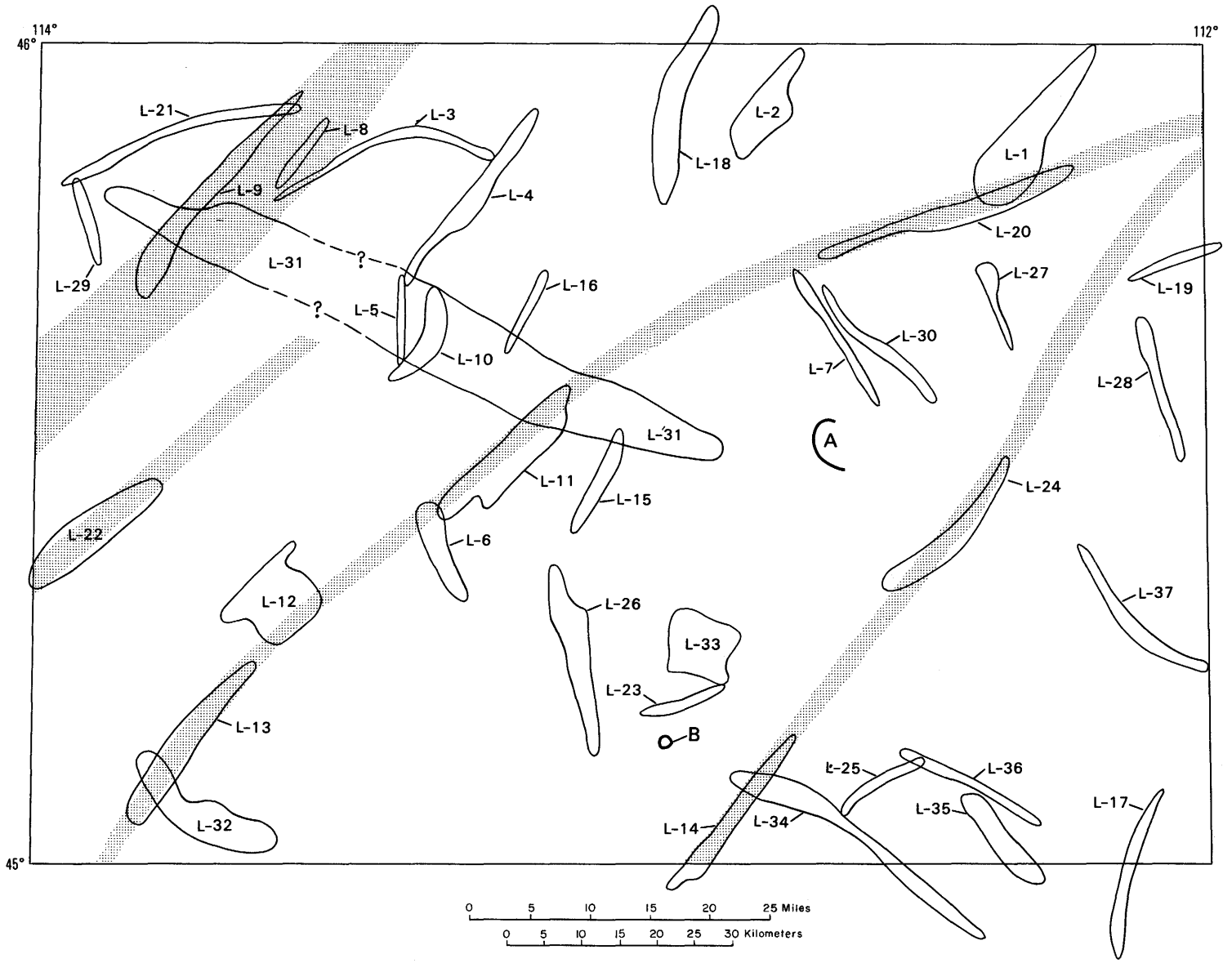

Figure 11.—Lineaments and arcuate features in the Dillon 1° × 2° quadrangle, Idaho and Montana. Stipple pattern indicates continuations of lineaments discussed in the text.

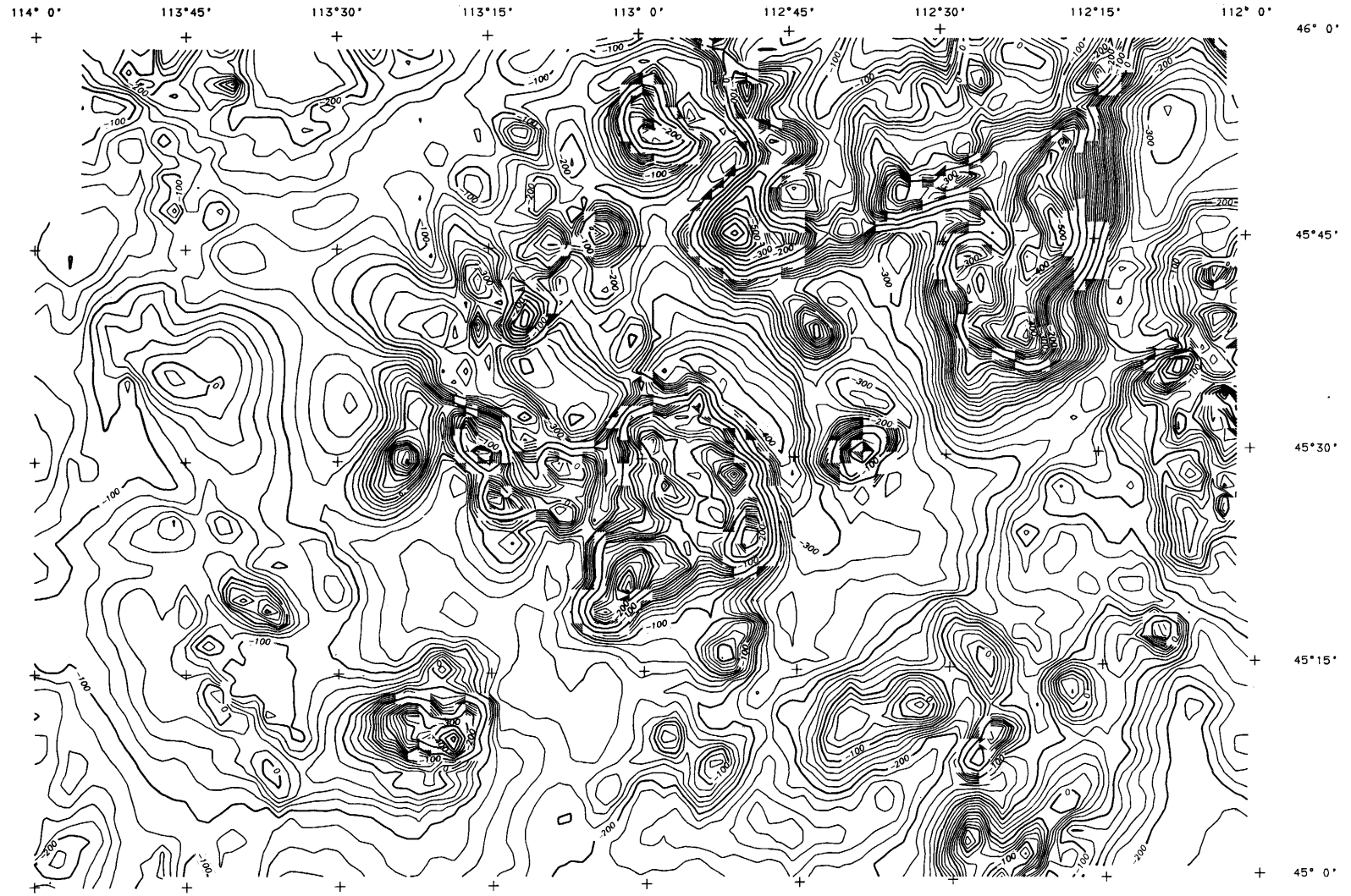

Figure 12.—Upward-continued aeromagnetic map of the Dillon 1° × 2° quadrangle, Idaho and Montana (W.F. Hanna, U.S. Geological Survey, unpub. data). Contour interval 20 gammas.

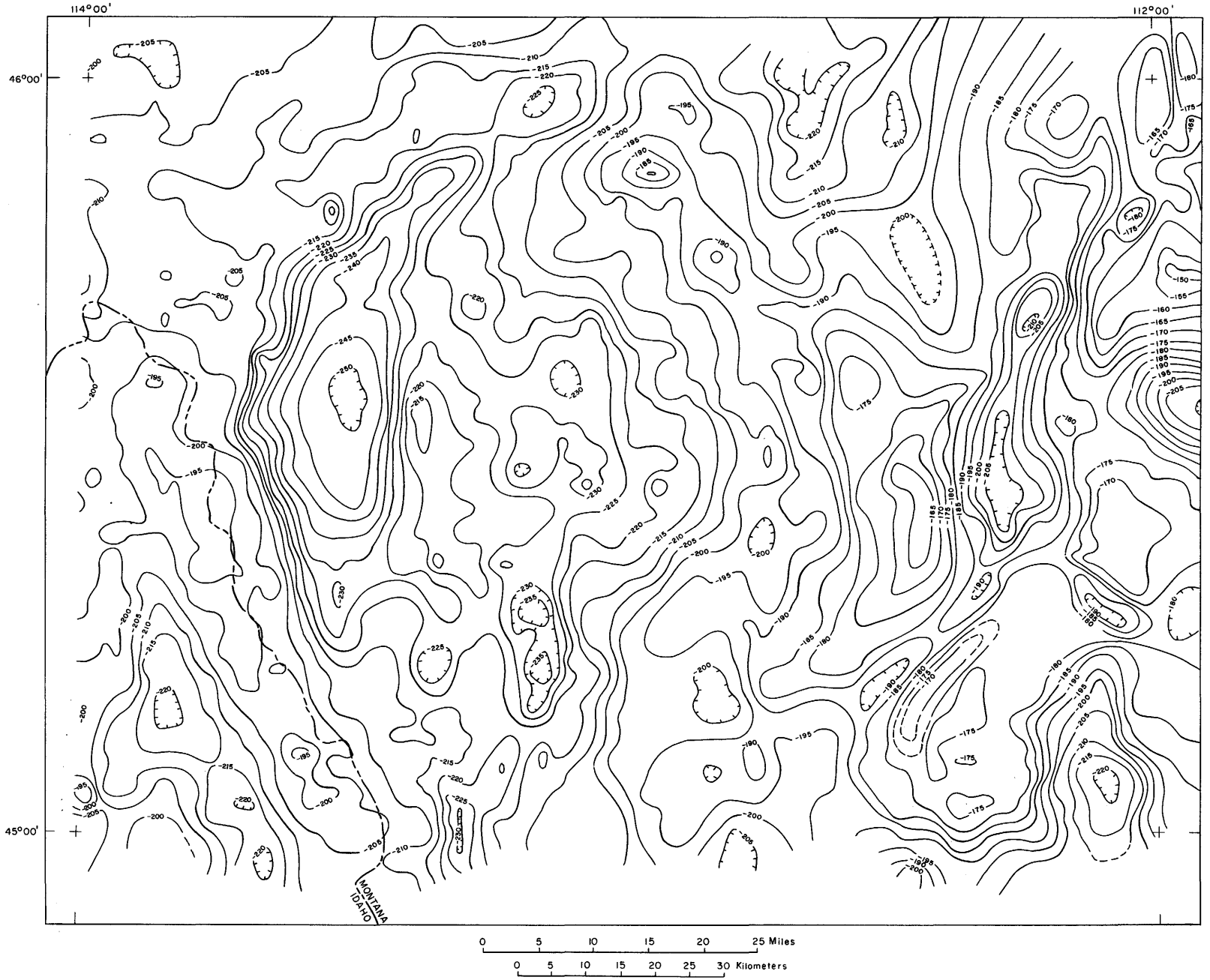

Figure 13.—Complete Bouguer gravity map of the Dillon 1° × 2° quadrangle, Idaho and Montana and vicinity (Kaufmann and others, 1983). Contour interval 20 milligals.

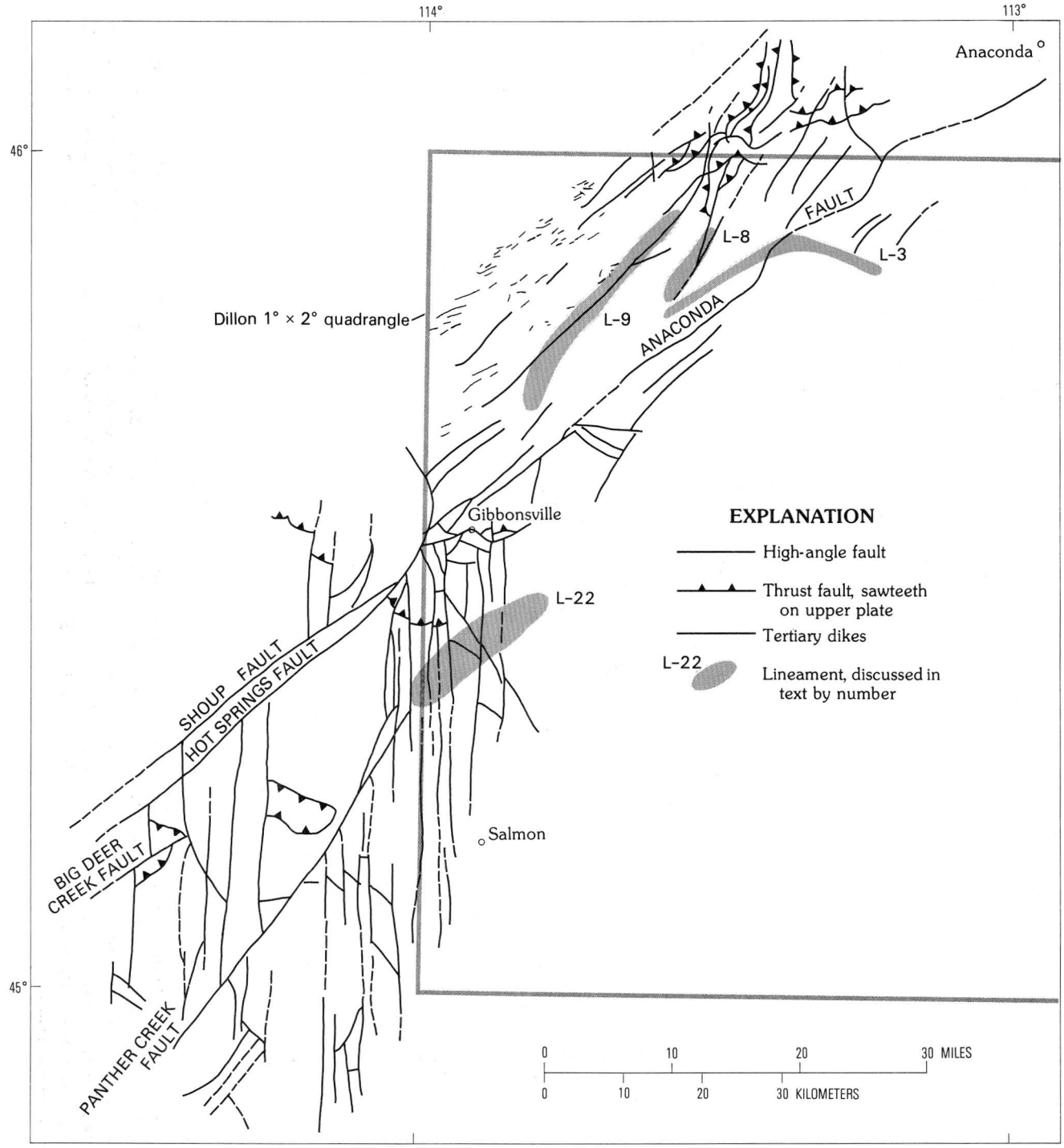

Figure 14.—Generalized structure map of the area between Salmon, Idaho and Anaconda, Montana showing the relationship of several lineaments. Modified from O'Neill and Lopez (1985).

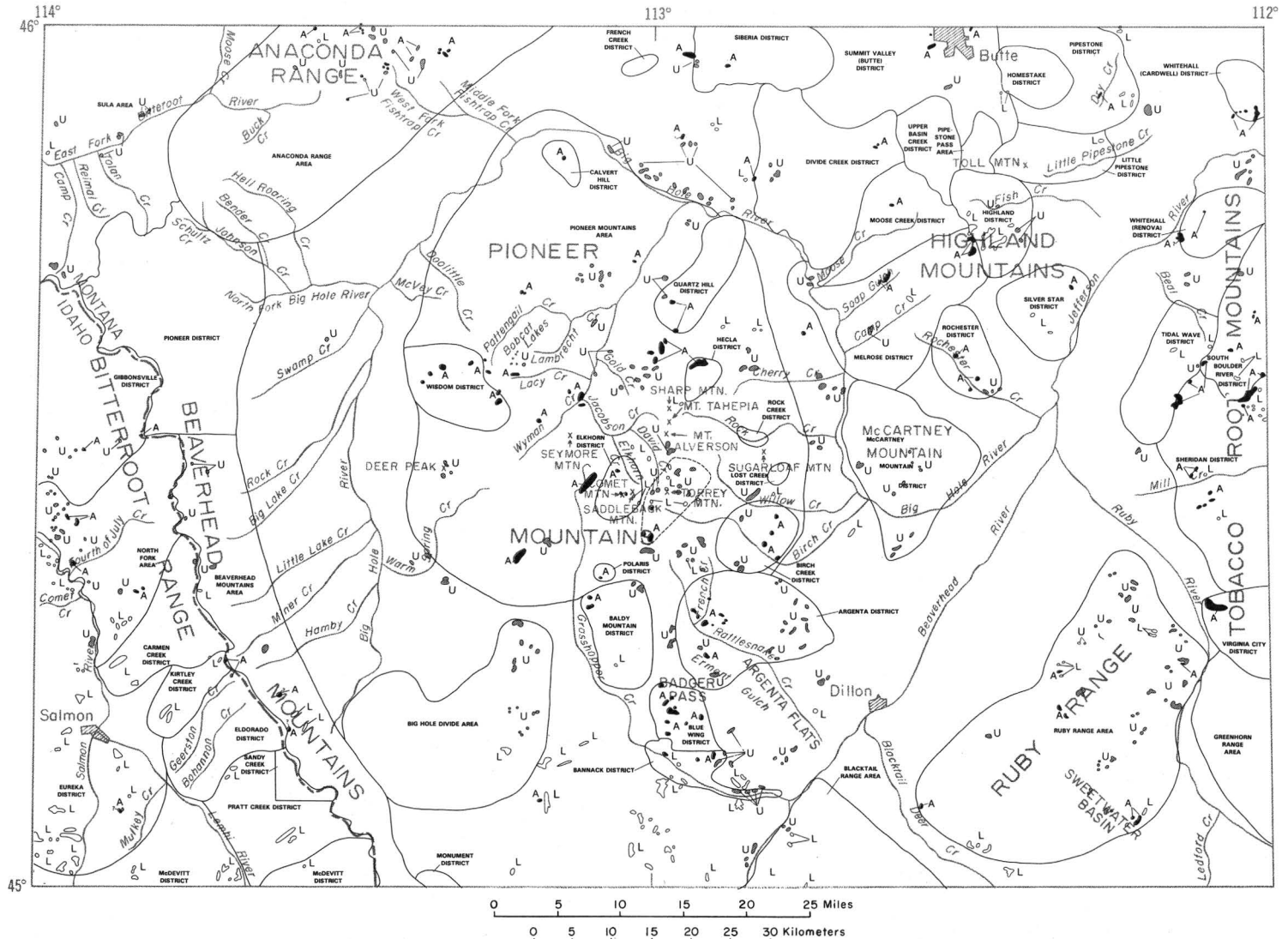

Figure 15.—Locations of hydrothermally altered rocks, unaltered limonitic rocks, and mining districts in the Dillon 1° × 2° quadrangle, Montana and Idaho (Segal and Rowan, 1989; Loen and Pearson, 1984). Symbols used: A–altered rocks, U–unaltered limonitic rocks, L–limonitic rocks which have not been evaluated in the field with respect to alteration. Heavy lines indicate boundaries of mining districts and mining areas; dashed line indicates boundary of an area which was identified in the alteration study (Segal and Rowan, 1989) and the geochemical data (B.R. Berger, U.S. Geological Survey, oral commun., 1983) as meriting further consideration.

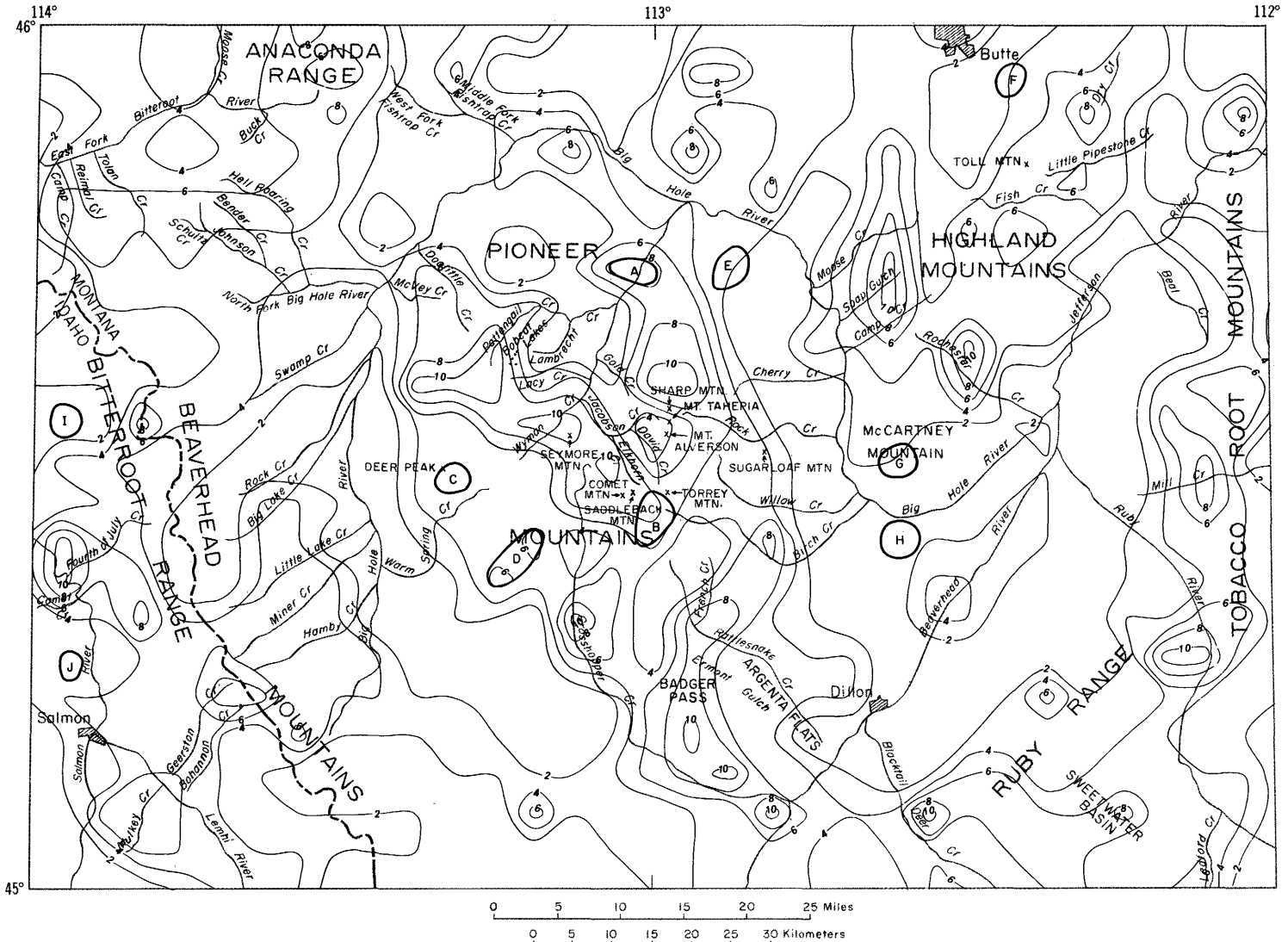

Figure 16.—Composite map showing the areal density of hydrothermally altered rocks, lineaments, N35°–58°E–trending linear features, and arcuate features gridded at a 5 km × 5 km spacing. Heavy solid lines indicate areas discussed in the pamphlet text. Values assigned to grid cells used to produce the composite map are shown in table 1.

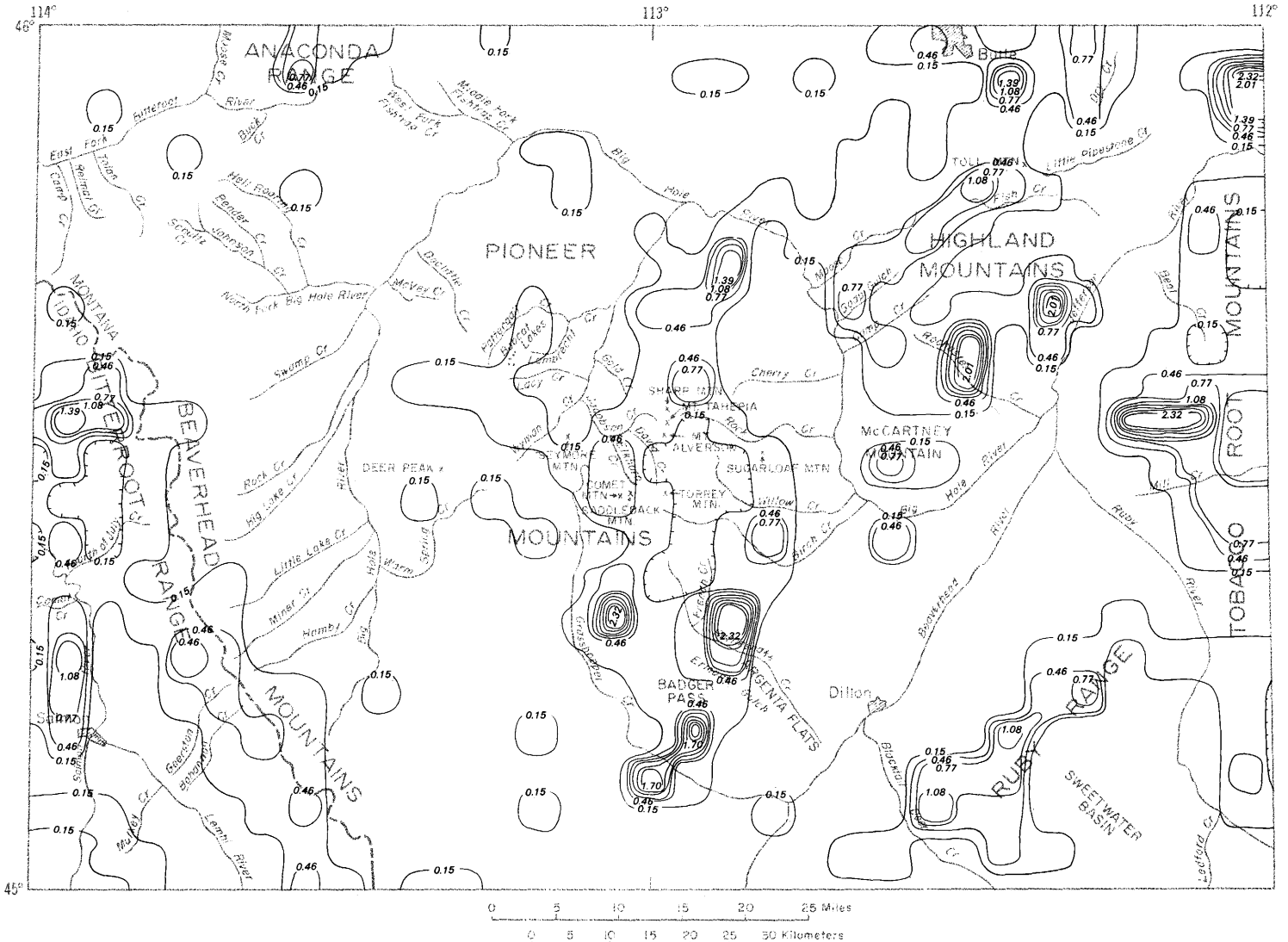

Figure 17.—Contour map showing the areal density of mines and prospects gridded at a 5 km × 5 km spacing in the Dillon 1° × 2° quadrangle, Idaho and Montana.

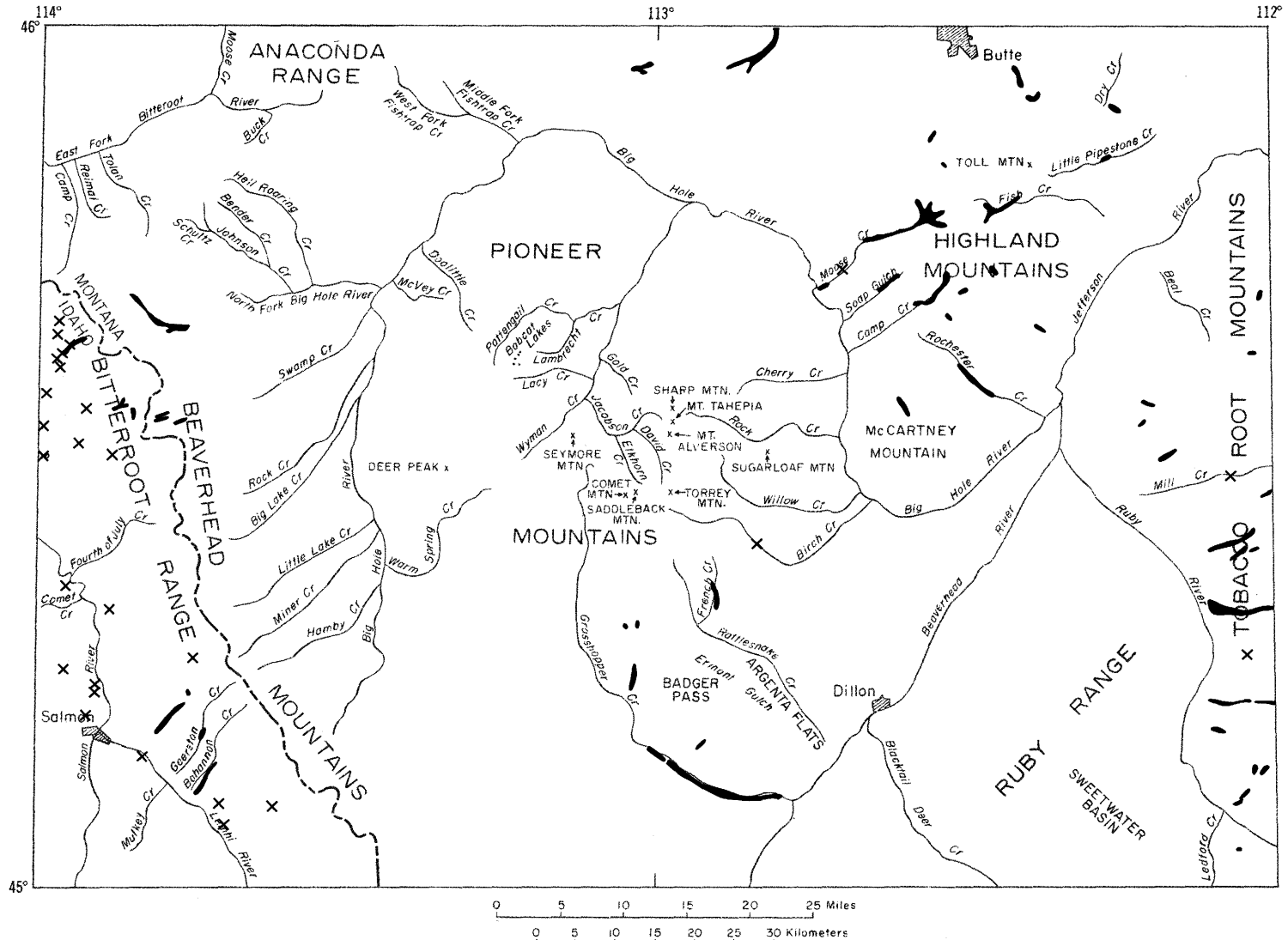

Figure 18.—Distribution of placer gold deposits in the Dillon 1° × 2° quadrangle, Idaho and Montana (from Loen and Pearson, 1984). Black areas show the approximate outlines of workings; × indicates extent of workings unknown or location only approximately known.

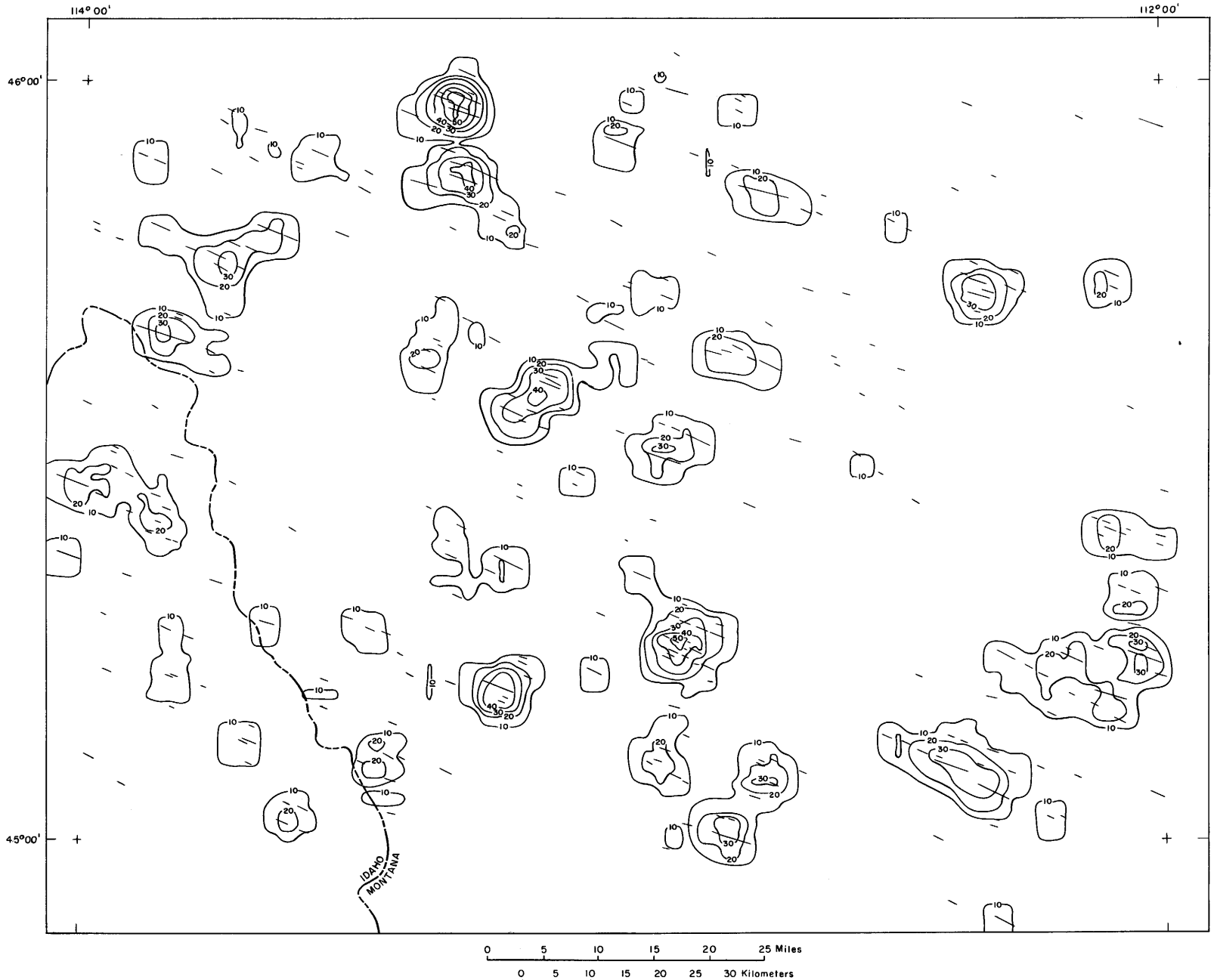

Figure A–1.—Contour map showing the areal density of N61°–75°W–trending linear features 1 km and longer from Landsat multispectral scanner (MSS) and side-looking airborne radar (SLAR) images in the Dillon 1° × 2° quadrangle, Idaho and Montana.

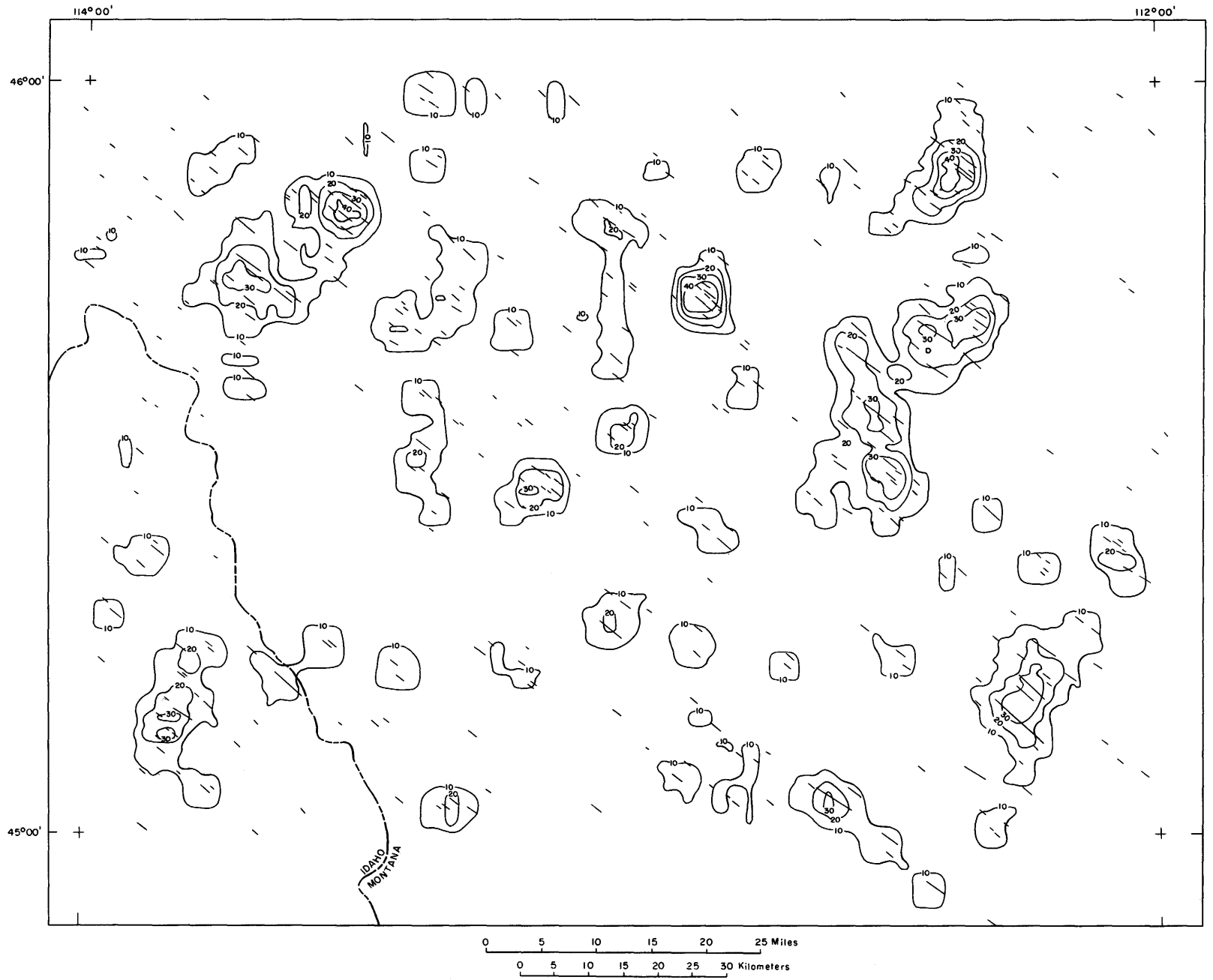

Figure A–2.—Contour map showing the areal density of N46°–58°W–trending linear features 1 km and longer from Landsat multispectral scanner (MSS) and side-looking airborne radar (SLAR) images in the Dillon 1° × 2° quadrangle, Idaho and Montana.

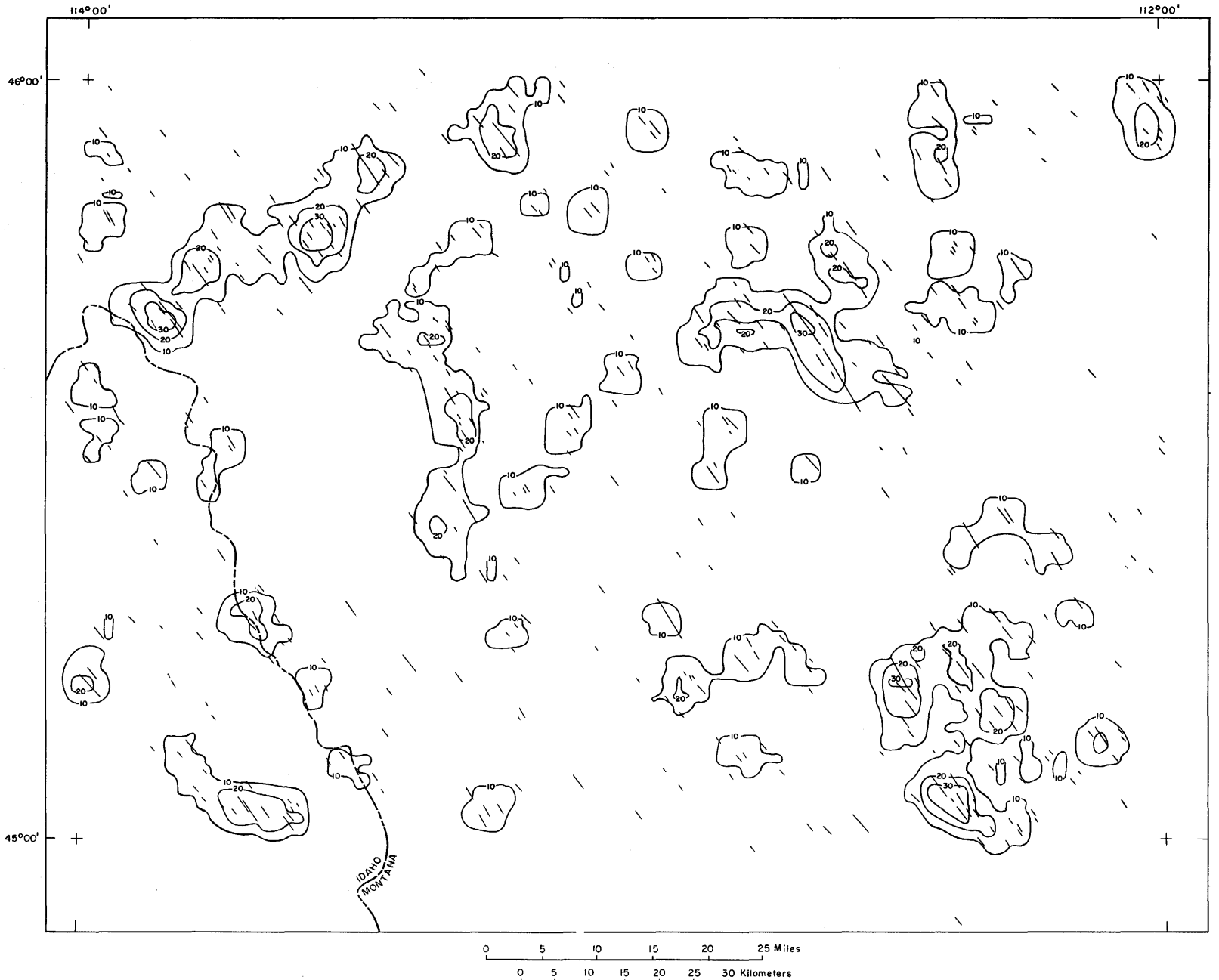

Figure A–3.—Contour map showing the areal density of N29°–44°W–trending linear features 1 km and longer from Landsat multispectral scanner (MSS) and side-looking airborne radar (SLAR) images in the Dillon 1° × 2° quadrangle, Idaho and Montana.

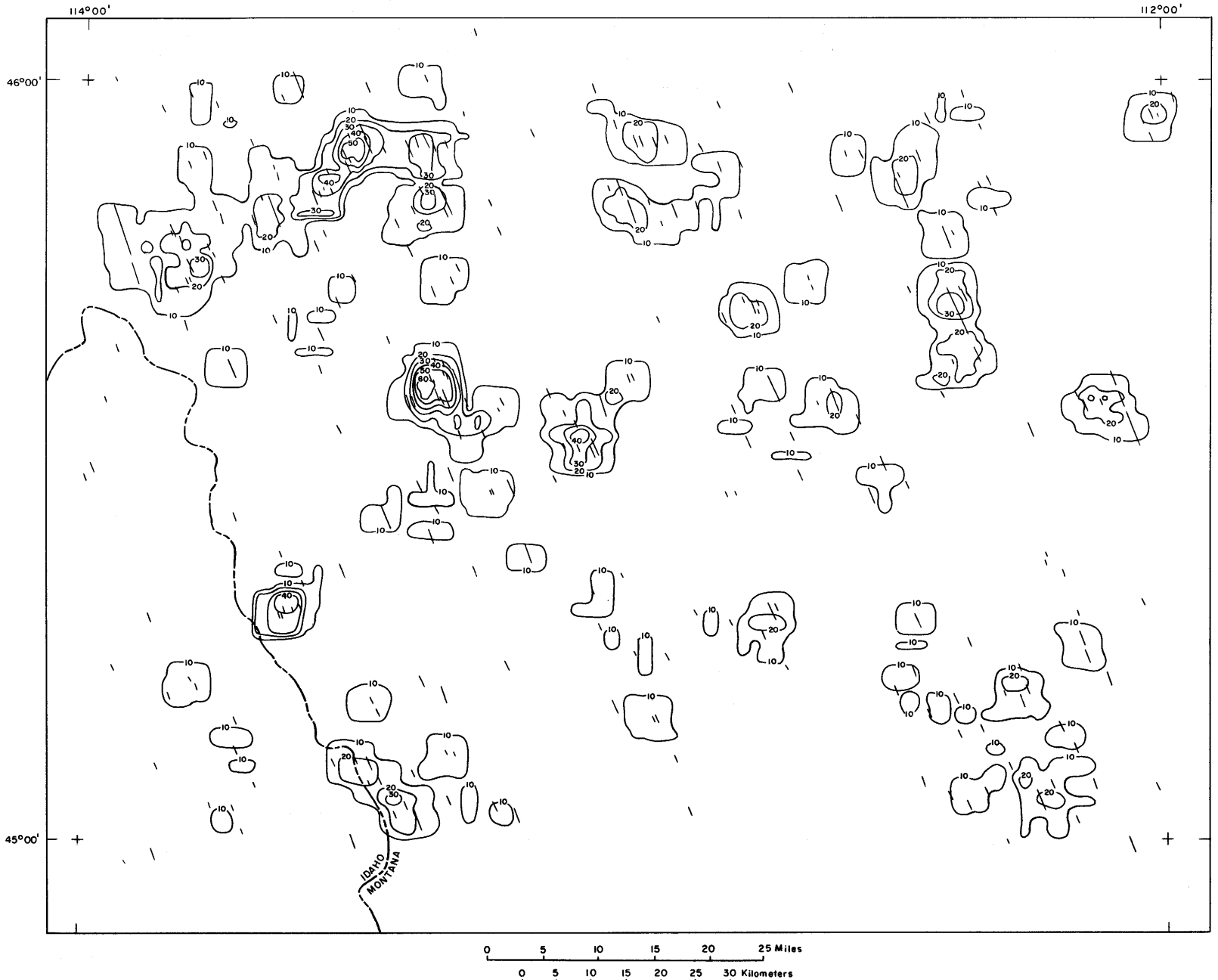

Figure A–4.—Contour map showing the areal density of N18°–27°W–trending linear features 1 km and longer from Landsat multispectral scanner (MSS) and side-looking airborne radar (SLAR) images in the Dillon 1° × 2° quadrangle, Idaho and Montana.

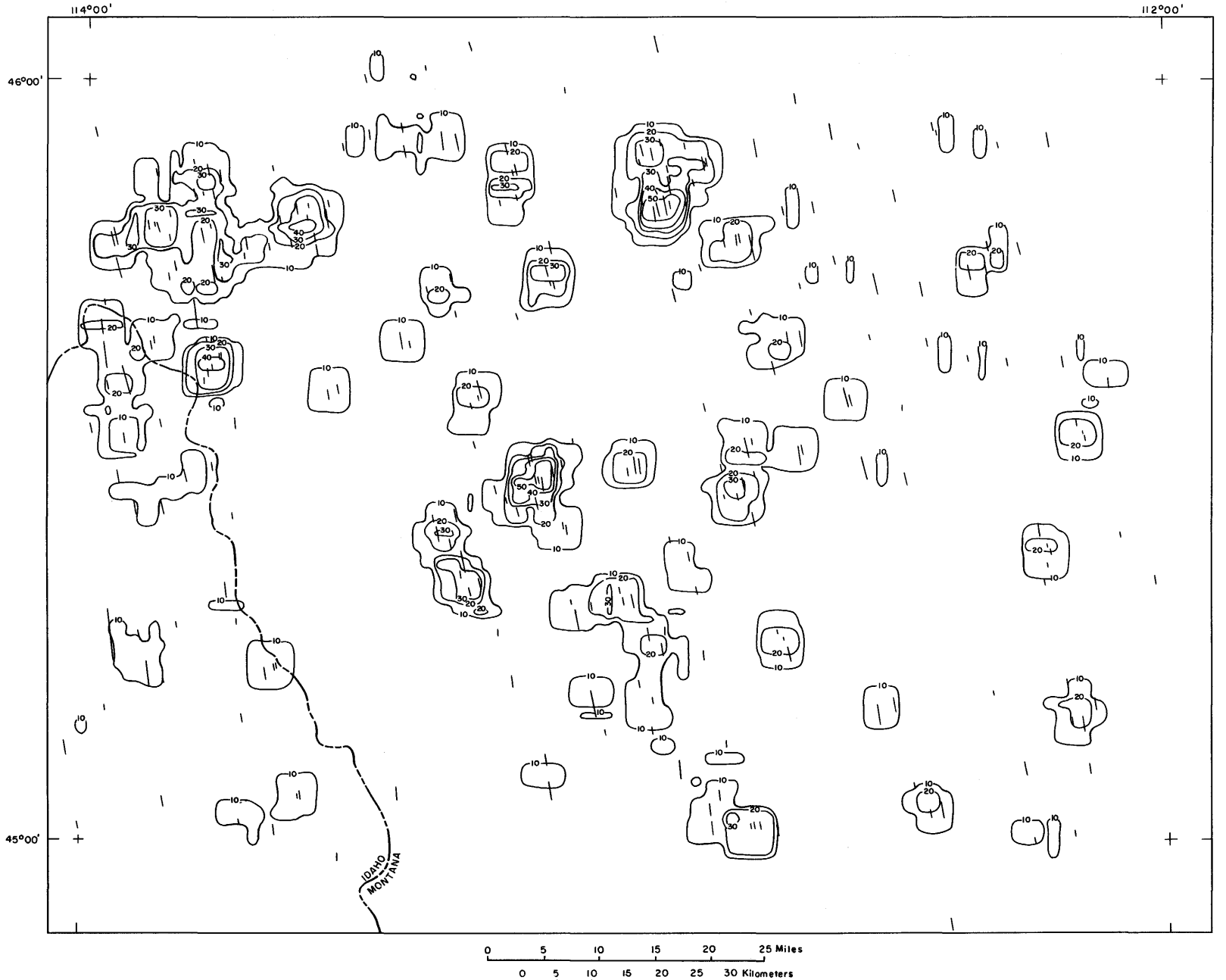

Figure A–5.—Contour map showing the areal density of N6°–15°W–trending linear features 1 km and longer from Landsat multispectral scanner (MSS) and side-looking airborne radar (SLAR) images in the Dillon 1° × 2° quadrangle, Idaho and Montana.

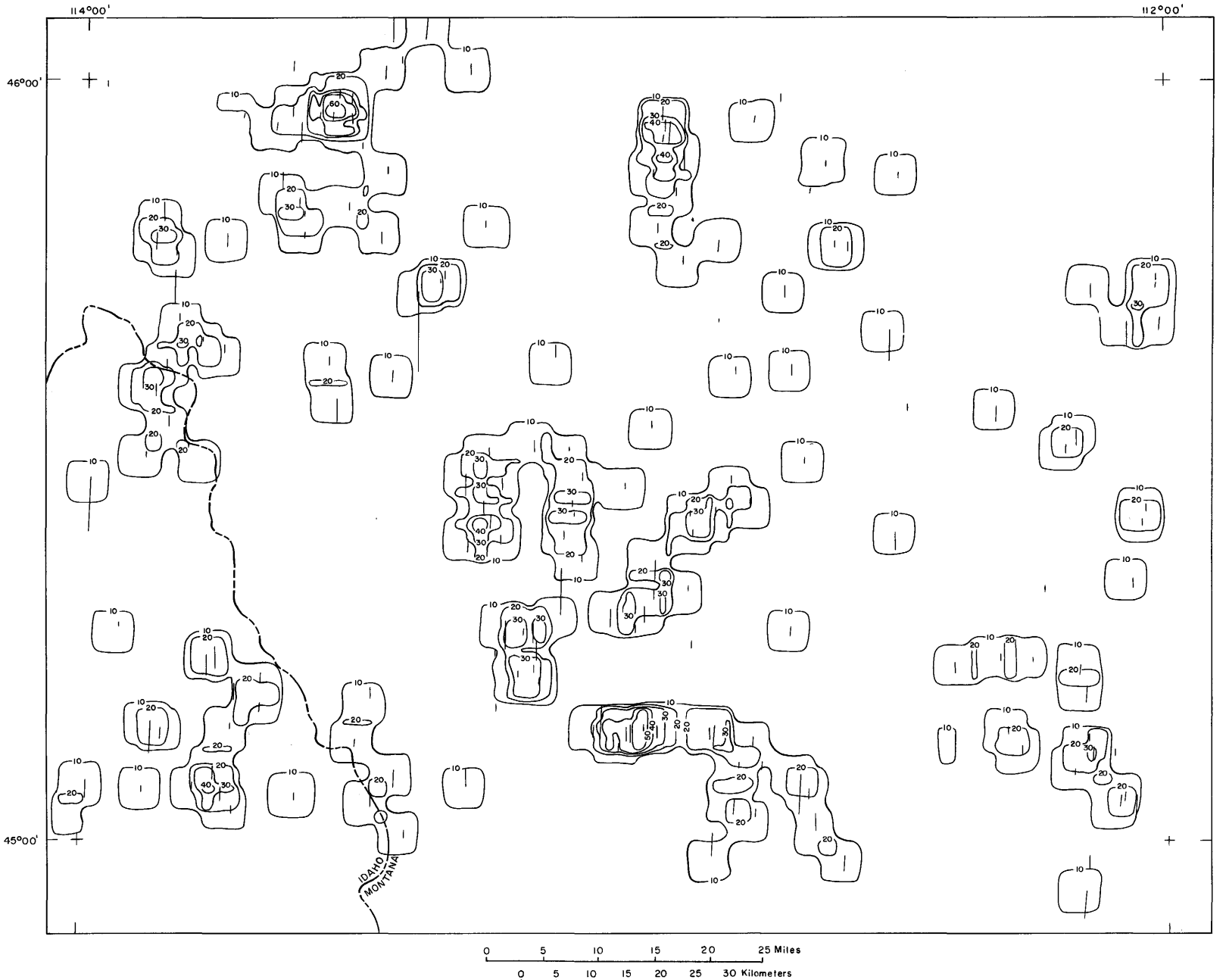

Figure A–6.—Contour map showing the areal density of N1°W–N–N4°E–trending linear features 1 km and longer from Landsat multispectral scanner (MSS) and side-looking airborne radar (SLAR) images in the Dillon 1° × 2° quadrangle, Idaho and Montana.

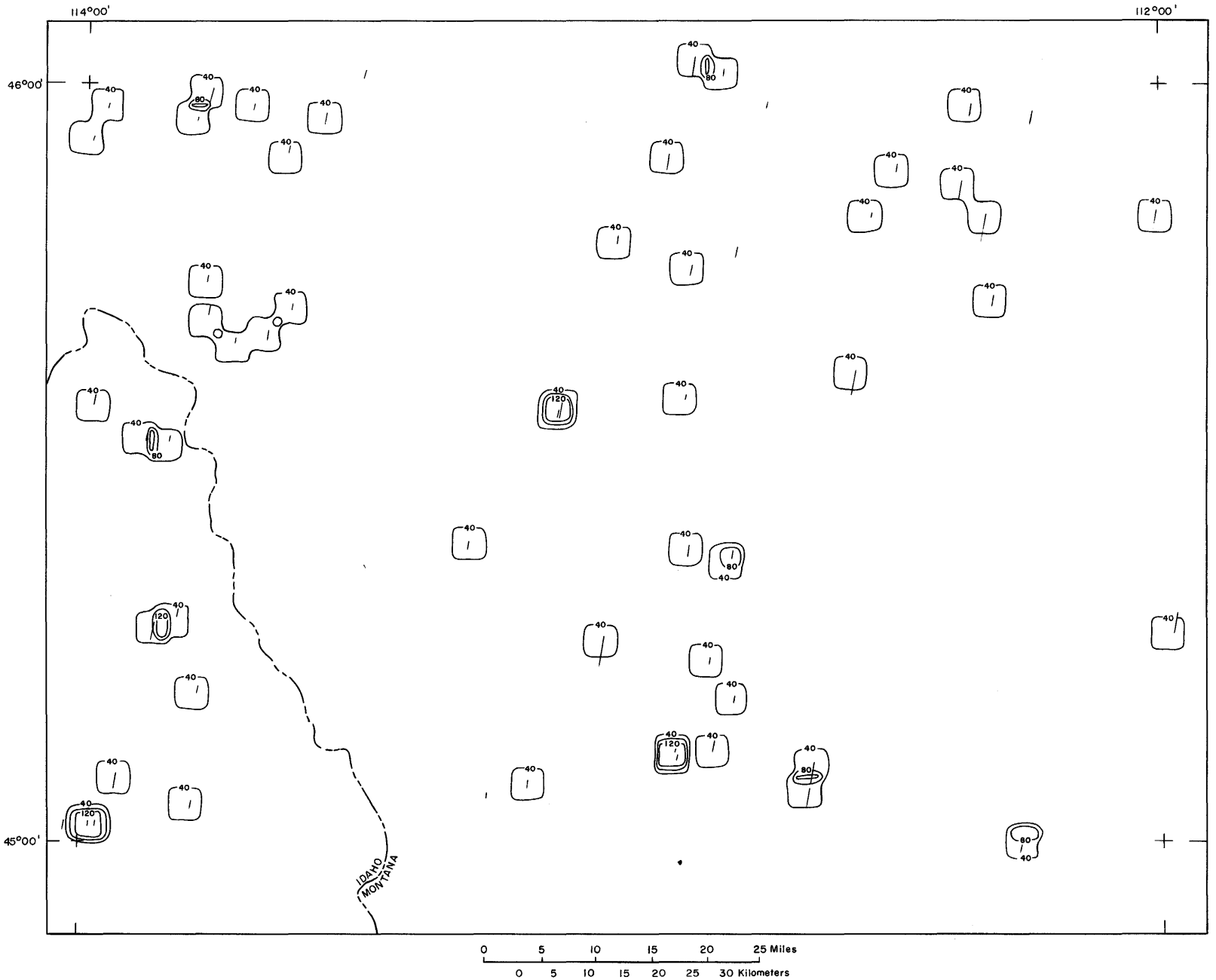

Figure A–7.—Contour map showing the areal density of N9°–10°E–trending linear features 1 km and longer from Landsat multispectral scanner (MSS) and side-looking airborne radar (SLAR) images in the Dillon 1° × 2° quadrangle, Idaho and Montana.

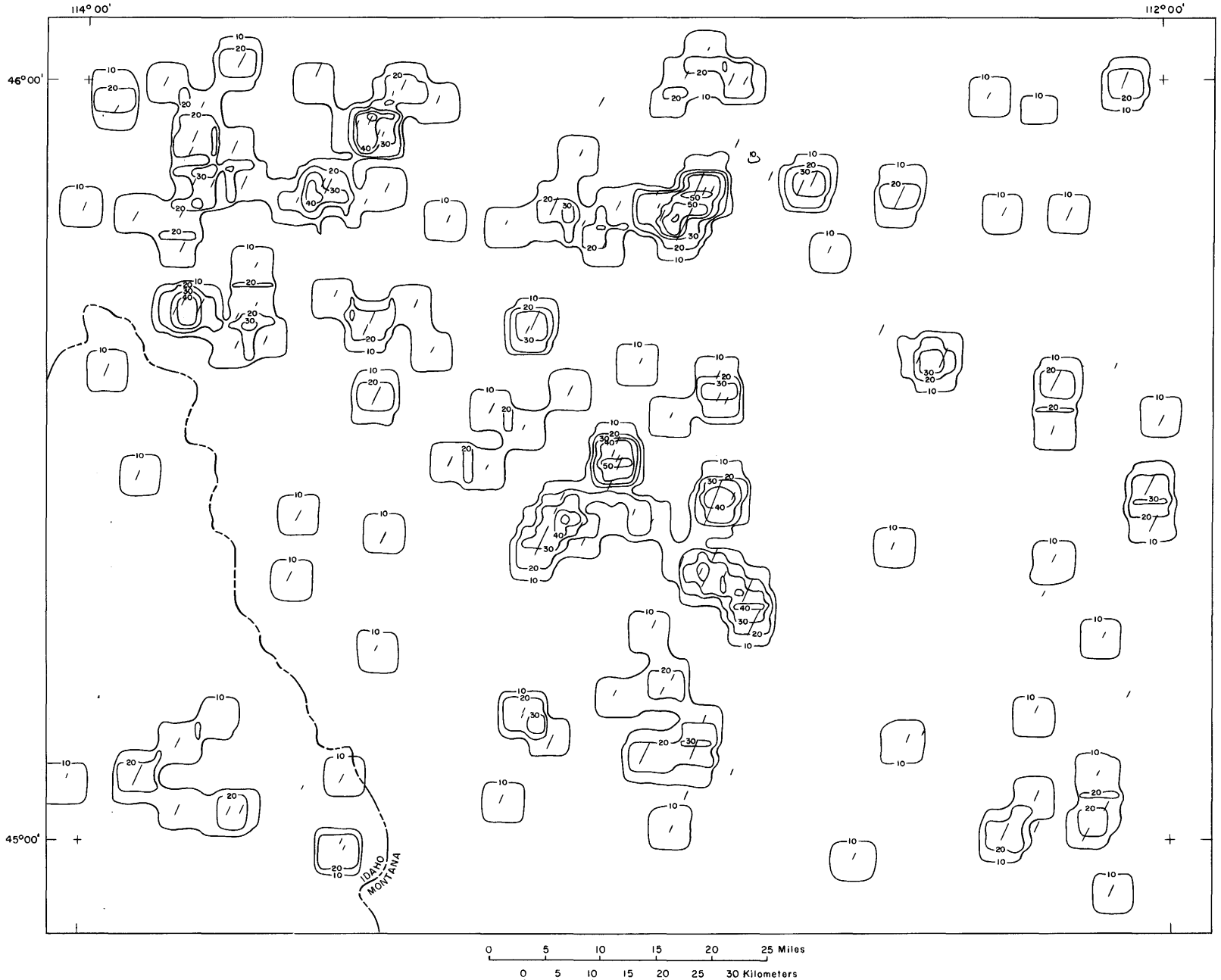

Figure A–8.—Contour map showing the areal density of N22°–26°E–trending linear features 1 km and longer from Landsat multispectral scanner (MSS) and side-looking airborne radar (SLAR) images in the Dillon 1° × 2° quadrangle, Idaho and Montana.

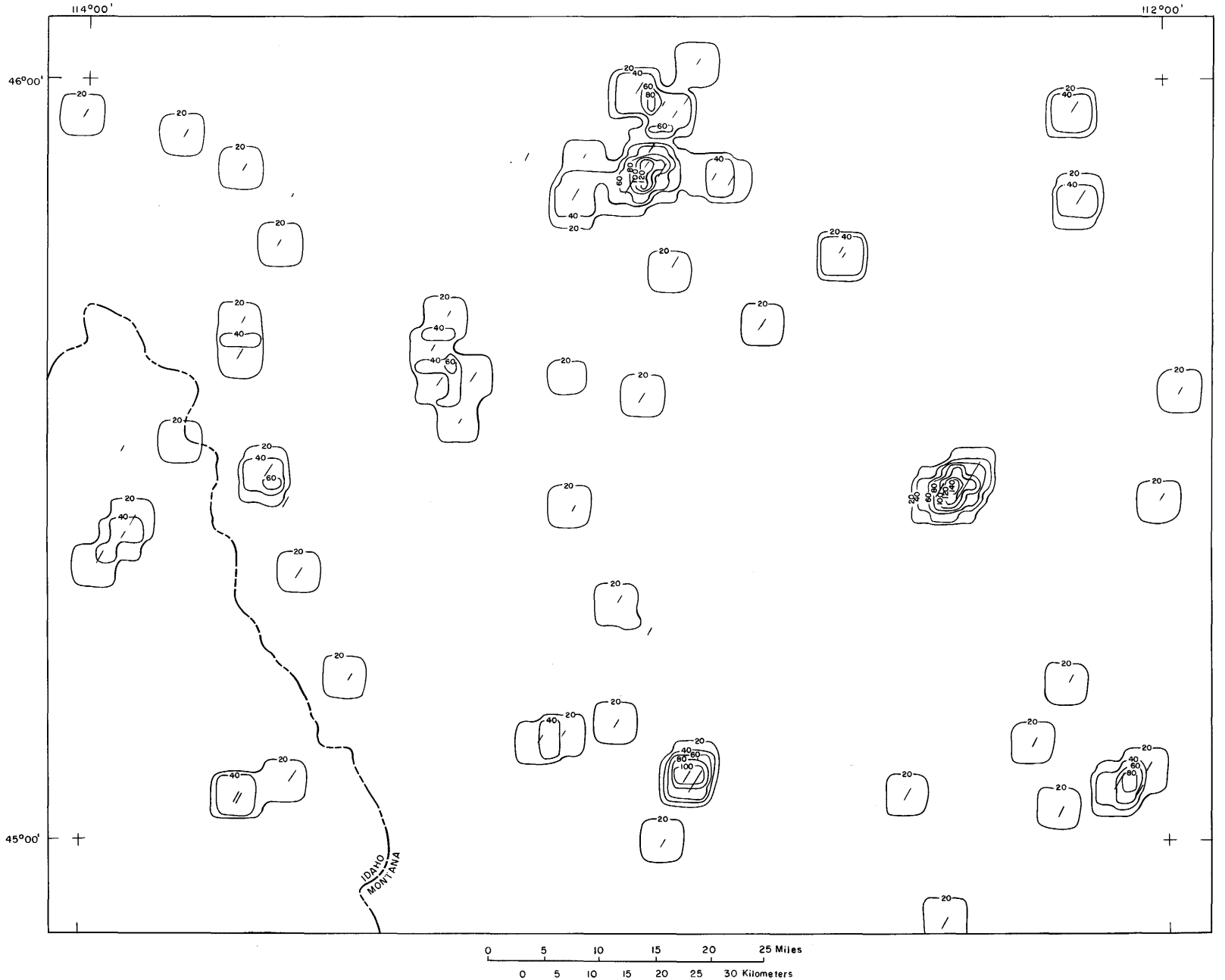

Figure A–9.—Contour map showing the areal density of N30°–31°E–trending linear features 1 km and longer from Landsat multispectral scanner (MSS) and side-looking airborne radar (SLAR) images in the Dillon 1° × 2° quadrangle, Idaho and Montana.

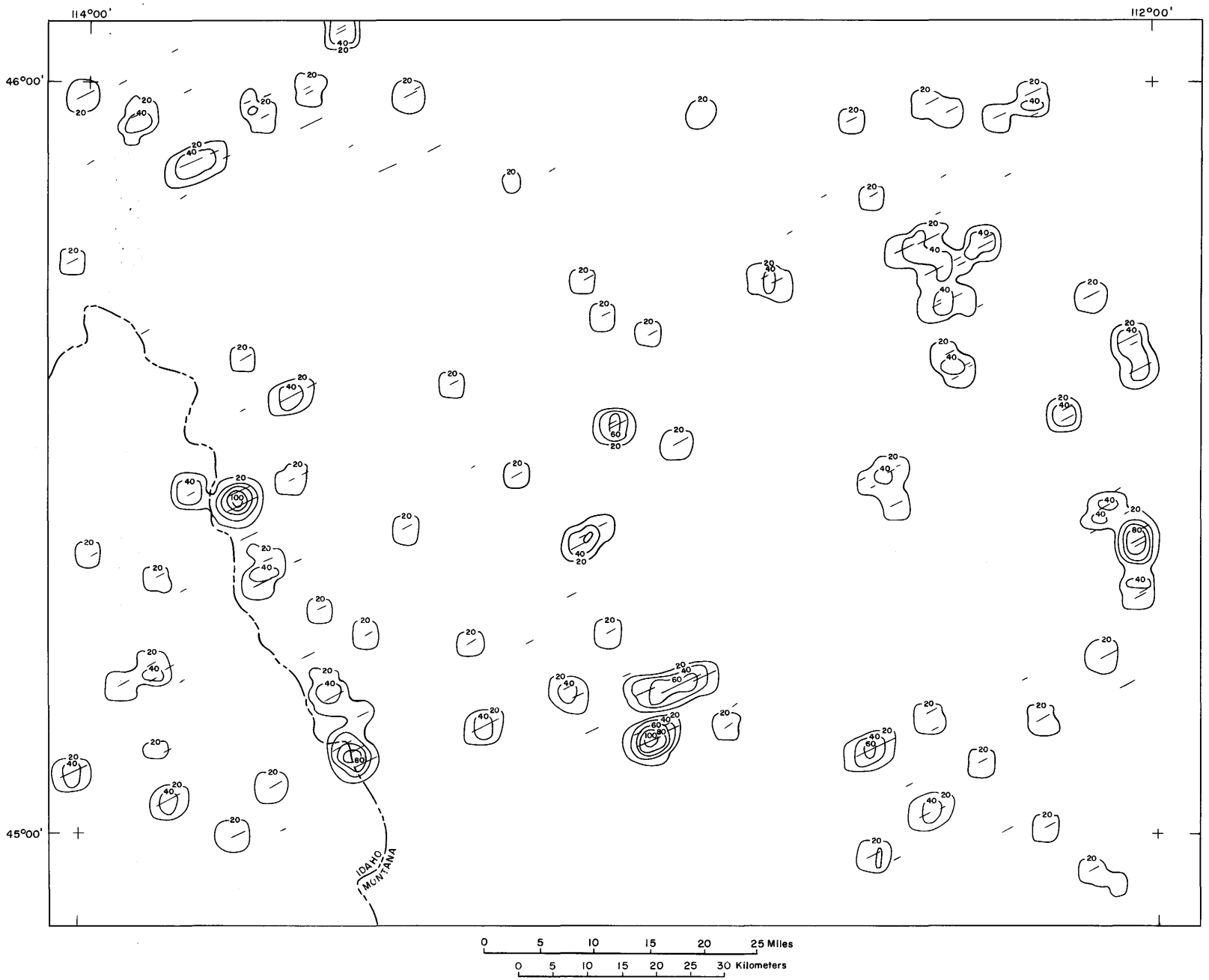

Figure A–10.—Contour map showing the areal density of N61°–65°E–trending linear features 1 km and longer from Landsat multispectral scanner (MSS) and side-looking airborne radar (SLAR) images in the Dillon 1° × 2° quadrangle, Idaho and Montana

U.S. GOVERNMENT PRINTING OFFICE: 1990 0–861-099